PAPER

Check for updates

Enhanced light absorption by ambient brown carbon aerosols in the eastern Himalayas

B. S. Arun, [ID] †[a] Mukunda M. Gogoi, [ID] *[a] Dhananjay Kumar Deshmukh, [ID] [a] Prashant Hegde, [ID] [a] Suresh Kumar Reddy Boreddy, [ID] [a] Arup Borgohain[b] and S. Suresh Babu[a]

This study investigates the light absorption properties of organic aerosols in PM_{10} collected at a high-altitude location (2700 m a.s.l.) in the eastern Himalayas from March 2019 to February 2020. The analysis reveals an enhanced light-absorbing signature of methanol-soluble brown carbon (MeS-BrC) extracts compared to water-soluble brown carbon (WS-BrC) within the optical wavelength range of 300–700 nm. MeS-BrC exhibits approximately twice the absorption compared to that of WS-BrC at 365 nm. The highest light absorption coefficients at 365 nm (b_{abs365}) are observed during spring for both MeS-BrC (9 ± 4.6 Mm^{-1}) and WS-BrC (5.9 ± 4.2 Mm^{-1}). Notably, the contribution of absorption from the water-insoluble fraction is relatively higher during the summer monsoon ($45.2 \pm 19.5\%$) and autumn ($44.1 \pm 18.4\%$). A significant linear relationship between WSOC and WS-BrC as well as OC and MeS-BrC at 365 nm suggests similar sources for BrC and WSOC (OC). Furthermore, significant positive correlations of b_{abs365} (WS-BrC and MeS-BrC) with the water-soluble fraction of total nitrogen (WSTN) and organic nitrogen (WSON) indicate the presence of nitrogenous organic chromophores playing a crucial role in BrC absorption during spring and autumn. The mass absorption efficiency at 365 nm (MAE_{365}) reveals that BrC in spring aerosols (WS-BrC: 1.5 ± 0.6 m^2 g^{-1}; MeS-BrC: 2.07 ± 0.8 m^2 g^{-1}) absorbs UV-visible light more efficiently compared to aerosols collected during other seasons. The enhanced MAE_{365} during spring resulted the highest simple forcing efficiency of 8.7 ± 3.9 W g^{-1} and 10.8 ± 5.2 W g^{-1} for WS-BrC and MeS-BrC, respectively, for a specific solar geometry and surface properties. This may be attributed to intense biomass burning followed by atmospheric processing of organic aerosols in the aqueous phase. These findings confirm the significant role of anthropogenic sources in enhancing BrC light absorption and radiative effects in this highly sensitive region of the eastern Himalayas. Such insights are crucial for devising effective strategies for mitigating climate change impacts in the Himalayan ecosystem.

Environmental significance

Studying light absorption properties of organic aerosols at remote high-altitude locations of the Himalayas is vital for understanding the radiative effects of absorbing aerosols influenced by anthropogenic sources located far from the pristine environment. This study investigates the light absorption properties, including its absorption coefficient, mass absorption efficiency, and imaginary refractive index, of both water-soluble and methanol-soluble brown carbon aerosols and brings out the signature of enhanced light absorption by BrC in a highly sensitive remote region of the eastern Himalayas.

1. Introduction

Carbonaceous aerosols (CA), which consist of organic carbon (OC) and elemental carbon (EC), are pervasive in the atmosphere. They are modulated by distinct origins either natural or anthropogenic,[1,2] which lead to complex interactions (scattering or absorption) with the solar radiation, and alter the energy balance of the Earth system.[3,4] CA also play a critical role in the formation of clouds *via* acting as cloud condensation nuclei and ice nuclei.[5,6] In this study, we focus primarily on the nature of OC and its light absorption properties in a remote high-altitude site in the eastern Himalayas. Knowing the important sources of organic aerosols present over the Himalayan region is essential for understanding the release of many organic compounds into the free-tropospheric environment, as sources of OC include biogenic volatile organic compounds (BVOCs) released by vegetation as well as emissions from biomass burning, fossil

[a]Space Physics Laboratory, Vikram Sarabhai Space Centre, Thiruvananthapuram 695022, India. E-mail: dr_mukunda@vssc.gov.in

[b]North Eastern Space Application Centre, Umiam 793103, India

† Currently at: Leibniz Institute for Tropospheric Research, Leipzig 04318, Germany.

fuel combustion, and industrial processes.[7,8] This is also useful to understand the atmospheric processing of organic aerosols *via* chemical reactions in the presence of atmospheric oxidants and solar radiation.[9,10]

Among the organic aerosols, there are specific components that have light-absorbing properties, referred to as brown carbon (BrC) aerosols. While EC absorbs light strongly over the entire wavelength spectrum,[11] BrC composed of a variety of organic compounds shows wavelength-dependent absorption characteristics.[3,4,12] BrC aerosols often absorb a substantial amount of light in the near UV and visible region of the electromagnetic spectrum.[13–15] However, the properties and composition of BrC are susceptible to alteration depending on emission sources, the aging processes of organic aerosols in the atmosphere, and the presence of co-emitted species such as SO_2, NOx, NH_3, *etc.*[16] There are several techniques used globally to understand the properties of BrC aerosols, including *in situ* measurements,[8,17–21] laboratory experiments,[22–25] and modeling studies[26,27] to quantify the light absorption contribution of organic aerosols, their sources and transformation as well as impacts on the atmosphere. Because of the light-absorbing nature of BrC, it contributes to the heating of the atmosphere, in addition to exerting various effects on photochemistry.[29]

The Himalayas and Tibetan Plateau (HTP), also referred to as the 'third pole', have the largest glacial reservoirs after the polar regions. It is also referred to as the "Water Tower of Asia" since it provides water to millions of people who live in downstream areas. As a result of its unique vulnerability to both human activity and climate change, HTP glaciers have experienced the greatest decline in recent decades.[30,31] Given that the HTP region is surrounded by the anthropogenic sources of South and East Asia, long-range transport of light-absorbing carbonaceous aerosols results in atmospheric warming over the region, which can influence the Asian monsoon system and accelerate the melting of glaciers through the deposition on snow and ice surface.[32,33] In the Himalayan region, the major contributor to atmospheric heating appears to be BC aerosols, which exert a greater impact on the climate than other chemical species. Nevertheless, a notable impact of light absorption attributed to BrC has been reported over a central Himalayan site.[34] However, despite its significance, there remains a need for a comprehensive understanding of BrC characteristics across the vast Himalayan region, particularly on the southern slope. This area receives intense solar radiation, leading to significant interactions between light-absorbing aerosols and solar energy, distinguishing it from other regions of the HTP.

As far as the light absorption due to atmospheric aerosols is concerned, previous studies over the Himalayas were mostly focusing on the characterization of BC[35–39] and mineral dust.[40,41] On the other hand, several studies were carried out in the Tibetan Plateau region[20,28,34,42–44] to understand the characteristics and evolution of BrC aerosols. In this context, the present study is unique in a way that they are characterized from an eastern Himalayan site "Lachung", where the environmental conditions such as altitude, surface properties, land use, vegetation, solar radiation and transport pathways differ substantially from those of the Tibetan Plateau.[45–50] Consequently, the

processes governing the dynamics of organic aerosol, their formation, transport and deposition as well as radiative implications are expected to be different. We focused on addressing this critical knowledge gap. Furthermore, Lachung holds significance due to its proximity to the Indo-Gangetic Plain (IGP), an aerosol hotspot in South Asia. Atmospheric transport from the IGP to the eastern Himalayas, coupled with regional emissions and atmospheric processing, significantly influences the aerosol composition and radiative properties in the eastern Himalayas.[51,52] These bear considerable implications, especially accelerated snow and glacier melting over the region.[53–57] In this context, we evaluated the year-round measurement of light-absorption characteristics of water-soluble and methanol-soluble BrC aerosols (WS-BrC and MeS-BrC) in PM_{10} collected during March 2019 to February 2020 from Lachung. We explored understanding the sources and atmospheric processing of BrC by examining the variability and interconnections between inorganic species along with organic carbon (OC), water-soluble OC (WSOC), and elemental carbon (EC). Based on this, we present the absorption coefficient, mass absorption efficiency and imaginary refractive index of WS-BrC and MeS-BrC aerosols. The relative light-absorption of BrC aerosols compared to EC aerosols as well as the simple forcing efficiency (SFE) of BrC aerosols is also presented. This study contributes valuable insights into the optical properties, sources, and radiative forcing of BrC, addressing a critical gap in understanding within the broader context of light absorption by organic aerosols.

2. Experimental details

2.1 Observational site and experimental set up

The aerosol samples were collected from Lachung (27.4 °N, 88.4 °E, ∼2700 m a.s.l.), a high-altitude remote mountainous site in the eastern part of the Himalayas (Fig. 1). Because of its unique geographical location, Lachung is an ideal site for investigating the composition, sources, and atmospheric processing of atmospheric aerosols. Mountains and densely forested areas surround the observational area. The site becomes heavily snow covered in the winter. Due to its high altitude and mountainous terrain, Lachung experiences pronounced seasonal variations in its meteorological conditions. More details about the experimental site and meteorological conditions are described elsewhere.[51,52]

A high-volume sampler (Model: APM 460 BL, Envirotech Instruments Pvt. Ltd., India) was used to collect PM_{10} ($D_a \leq 10$ μm) samples in pre-combusted quartz fiber filters (20 × 25 cm², Pallflex 2500QAT-UP) from March 2019 to February 2020 at a constant flow rate of 1 ± 0.1 m³ min⁻¹, which covers all seasons over the sampling site. A total of 73 PM_{10} samples were collected during the sampling period. The collected samples were then classified into spring (March–May, $n = 18$), summer (June–September, $n = 16$), autumn (October–November, $n = 18$) and winter (December–February, $n = 21$). Several field blanks were collected under similar sampling conditions as those of aerosol filter samples during the study period to correct the background or handling contamination.

© 2024 The Author(s). Published by the Royal Society of Chemistry

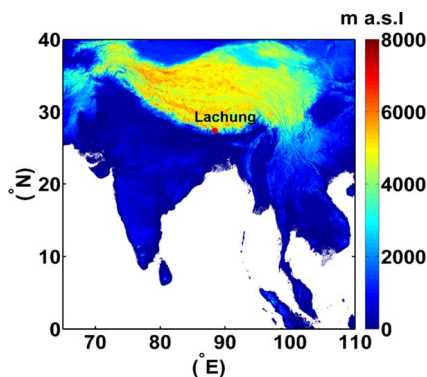*Environ. Sci.: Atmos.*, 2024, **4**, 782–801 | **783**

Fig. 1 Geographic location of the Lachung observational site (27.4 °N, 88.4 °E, 2700 m a.s.l.) in the eastern part of the Himalayas.

2.2. The light-absorbing properties of BrC

A UV-visible spectrophotometer (Agilent Carry 4000) was used to obtain the light absorption spectra of BrC across a wavelength range of 300–700 nm.[34] For this, WS-BrC and MeS-BrC were extracted from separate filter punches (6.28 cm^2) via ultra-sonication for 30 min with 10 mL Milli-Q water and 10 mL methanol, respectively. The water and methanol extracts were then filtered to eliminate insoluble particles and filter debris using 0.22 μm polyether sulphone (PES) and 0.45 μm poly-tetrafluoroethylene (PTFE) disc filters, respectively. Here, we followed the methodology as described in earlier studies,[58,59] obtaining good extraction efficiency of BrC chromophores. Paraskevopoulou et al. (2023 a,b)[59,60] also reported several other techniques for assessing extraction of BrC, encompassing both direct and indirect methodologies. It is noteworthy that the indirect approach employed in our present investigation bears a limitation in attributing the entirety of MeS-BrC to OC.

The absorption coefficients (Mm^{-1}) of WS-BrC and MeS-BrC were calculated using the following equation described in Wu et al.[20]

$$b_{\text{abs}\lambda} = (A_\lambda - A_{700}) \frac{V_1}{V_a \times L} \times \ln(10) \quad (1)$$

where A_λ and A_{700} are the light-absorbance of the extracts at the wavelength λ and 700 nm, respectively. V_1 represents the volume of the solvent used for the extraction of the filter sample, and V_a refers to the air volume corresponding to the extracted filter area used for the analysis. L is the optical path length. ln(10) is used to convert the log base-10 records of data to a natural log, which is typical in the records of atmospheric measurement results. According to previous studies,[61,62] the absorption coefficient at 365 nm is usually used for light-absorption of BrC to avoid disturbance of inorganic components such as nitrate. The mass absorption efficiency (MAE, m^2 g^{-1}) of both WS-BrC and MeS-BrC at a given wavelength is described by using the following equations.

$$\text{MAE}_{\text{WS-BrC}} = \frac{b_{\text{abs}\lambda}}{\text{WSOC}} \quad (2)$$

$$\text{MAE}_{\text{MeS-BrC}} = \frac{b_{\text{abs}\lambda}}{\text{OC}} \quad (3)$$

where WSOC and OC are the concentrations of WSOC and OC in PM$_{10}$ samples. It is noteworthy that the current MAE estimates are likely underestimated due to the attribution of the whole OC mass to MeS-BrC. Previous studies[11,63] have suggested that MeS-BrC could represent nearly 85–90% of the OC mass. However, recent studies[59,60] which used a modified or direct approach have revealed an even potentially further lower proportion, with MeS-OC mass accounting for about 68–72% of the OC mass. Thus, the indirect estimation methods utilized for MeS-BrC assessment in the present study differ from more efficient direct methodologies to estimate the absorption of MeS-BrC.[59] However, numerous studies have quantified methanol-soluble OC concentrations using an indirect method, which involves determining the OC fraction remaining on filters after methanol extraction and then subtracting it from the total OC. This approach is prone to overestimating MeS-OC due to the detachment and transfer of insoluble OC into methanol extracts.[64]

The wavelength dependence of light absorption with respect to the empirically defined power-law relationship is described by using the following equation defined in Laskin et al.[3]

$$\text{MAE}_{\text{WS-BrC}} = K\lambda^{-\alpha} \quad (4)$$

$$\text{MAE}_{\text{MeS-BrC}} = K\lambda^{-\alpha} \quad (5)$$

where K is a factor that includes aerosol mass concentrations and α denotes the absorption Ångström exponent (AAE). We determined the AAE of WS-BrC and MeS-BrC in the samples by using a linear regression of $\log(b_{\text{abs}\lambda})$ versus $\log(\lambda)$ over a wavelength range of 300–450 nm. Utilizing MAE values, the imaginary part of the complex refractive index of BrC was obtained using the following equations.

$$k_{(\lambda\text{-BrC\_H}_2\text{O})} = \frac{\rho\lambda b_{\text{abs}\lambda}}{4\pi \times \text{WSOC}} = \frac{\rho\lambda\text{MAE}}{4\pi} \quad (6)$$

$$k_{(\lambda\text{-BrC\_MeOH})} = \frac{\rho\lambda b_{\text{abs}\lambda}}{4\pi \times \text{OC}} = \frac{\rho\lambda\text{MAE}}{4\pi} \quad (7)$$

where ρ is the particle density (assumed to be 1.5 g cm^{-3}; Bikkina and Sarin.[65]). The above relations are formulated based on Mie theory with the assumption that particles were of spherical morphology and externally mixed with other light-absorbing components.[66] More details about Mie calculations can be found in Liu et al.[66]

2.3 Light attenuation in the atmosphere

The light absorption by WSOC or OC is estimated to be a product of the solar emission flux and the attenuation of light by WSOC or OC integrated over a broad wavelength range between 300 and 2500 nm. The wavelength dependent solar spectral irradiance (I_0) is obtained through the clear sky Air Mass 1 Global Horizontal (AM1GH) solar irradiance model.[67] The light attenuation in the atmosphere by an absorbing species, including WSOC, OC and EC, can be estimated using the following equation proposed by several authors (Kirillova et al.,[61] Alang et al.,[68] Wu et al.,[58] and Srinivas et al.[62]).

$$\frac{I_0 - I}{I_0} = 1 - e^{-\left(\sigma_x \times \left[\frac{\lambda_0}{\lambda}\right]^\alpha C_x h_{ABL}\right)} \quad (8)$$

where σ_x refers to mass absorption efficiency ($m^2\ g^{-1}$) for the absorbing species X such as WSOC, OC, and EC. C_x and h_{ABL} correspond to the mass concentration of absorbing species and atmospheric boundary layer height, respectively. Following eqn (8), the fractional contribution of solar absorption by WSOC or OC relative to EC is estimated as (Alang *et al.*,[68] Wu *et al.*,[58] Srinivas *et al.*,[62] Bikkina and Sarin,[65] and Kirillova *et al.*[34]),

$$f = \frac{\int_{300}^{2500} I_0(\lambda)\left[\frac{I_0 - I}{I_0}(\lambda, \text{WSOC})\right]d\lambda}{\int_{300}^{2500} I_0(\lambda)\left[\frac{I_0 - I}{I_0}(\lambda, \text{EC})\right]d\lambda} \quad (9)$$

The MAE of EC (σ_{EC}) was estimated from the attenuation measured using an aethalometer during the study period as reported in Arun *et al.*[51] along with the concentration of EC measured using an OC-EC analyzer as per the procedure previously reported by Ram and Sarin.[69]

The simple forcing efficiencies (SFE) of WS-BrC and MeS-BrC were estimated using the methodologies available elsewhere (Lei *et al.*,[70] Srinivas *et al.*,[62] Alang *et al.*,[68] and Bikkina and Sarin[65]),

$$\frac{dSFE_{BrC}}{d\lambda} = a_s \times T_{atm}^2 \times (1 - F_c) \times MAE_{\lambda BrC} \times \frac{dS(\lambda)}{d\lambda} \quad (10)$$

In the above equation, $dS(\lambda)/d\lambda$ is the wavelength-dependent variation in the solar irradiance.[53] a_s and T_{atm} denote surface albedo and atmospheric transmission, respectively. F_c corresponds to the fraction of cloud cover. The surface albedo values ($\sim$0.21, 0.19, 0.19, and 0.18 during winter, spring, summer and autumn, respectively) were taken from GLDAS VIC Land Surface Model L4 monthly 1.0 $\times$ 1.0-degree V2.1 (GLDAS_VIC10_M) products. The cloud fractions (F_c in % $\sim$64, 78, 88, and 65) were obtained from CMSAF cLoud, Albedo and the RAdiation dataset (AVHRR based CLARA-A3, Karlsson *et al.*[71]). The values of T_{atm} ($\sim$0.7862, 0.0.7443, 0.7692 and 0.8016) were calculated using Simple Model of the Atmospheric Radiative Transfer of Sunshine (SMARTS). Following this, SFE is estimated in W g^{-1} for different seasons by integrating the aforementioned equation for the wavelength range of 300–700 nm.

2.4. Measurements of OC, EC, WSOC, WSTN and water-soluble inorganic ions

To support the inferences from the BrC measurements, we used chemical composition data measured from the same filter samples that we had already reported in our earlier studies.[51,52] Briefly, OC and EC in PM_{10} samples were analyzed by using an OC-EC analyzer (Sunset Laboratory, Inc.) following the National Institute of Occupational Safety and Health (NIOSH) thermal-optical transmittance (TOT) protocol.

WSOC and water soluble total nitrogen (WSTN) were measured using a total organic carbon and nitrogen analyzer

(Model: TOC-L_CPH) in conjunction with an auto sampler (Model: ASI-L) from Shimadzu, Japan. Briefly, three to four filter punches of sample filter area (3.14 cm²) were extracted in 50 mL Milli-Q water (specific resistance: 18.2 MΩ) under ultrasonic agitation for 30 min. The sample extracts were then filtered using a syringe filter of a 0.22 μm pore size. The filtered liquid sample was then injected into the instrument for analysis using the autosampler. The total carbon content in the sample, referred to as water-soluble total carbon (WSTC), and water-soluble inorganic carbon (WSIC) were estimated separately in two distinct steps using a non-dispersive infrared (NDIR) detector. WSOC was then calculated by subtracting WSIC from WSTC. The nitrogen content in the same sample extract (WSTN) was analyzed with an ozone chemiluminescence detector.

Water soluble ionic components were measured by using an ion chromatograph (Metrohm, Switzerland). Water-soluble organic nitrogen (WSON) was estimated by subtracting WSIN from the WSTN. The field blanks collected during the measurement period were also analysed, and blank corrections were made to acquire the actual levels of the individual chemical species. Further details of the analysis techniques for the analyses of OC, EC, WSOC, WSTN, and water-soluble ions are given elsewhere.[41,51,52,72]

3. Results and discussion

3.1 Light absorption by brown carbon in the water and methanol extracts

Fig. 2(a) shows the temporal evolution of the absorption coefficients (b_{abs365}) for WS-BrC and MeS-BrC at Lachung during the study period. b_{abs365} varied from 0.58 to 18.2 Mm^{-1} for WS-BrC and 1.79 to 20 Mm^{-1} for MeS-BrC. Higher light absorption by BrC was found during spring and winter (Table 1), whereas the lowest absorption was found during the summer monsoon period. The light absorption by methanol extracts at 365 nm was 1.7 times higher than that measured by water extracts, indicating that methanol extracts more brown carbon chromophores than water which lead to higher b_{abs} values.

Fig. 2(a) also shows the temporal evolution and seasonal values of the water-insoluble fraction of BrC. In this study, we employed the methodology delineated by Satish and Rastogi[19] to assess the proportional impacts of water-insoluble constituents. This is presented as

$$\text{Water-insoluble BrC (\%)} = \frac{b_{abs\_methanol} - b_{abs\_water}}{b_{abs\_methanol}} \times 100 \quad (11)$$

The seasonal changes in the % of water-insoluble BrC were found to be higher during the summer monsoon (45.2 ± 19.5%) and autumn (44.1 ± 18.4%) period, respectively. The lowest fractions of insoluble BrC observed during spring indicated the dominant absorption of light due to water-soluble chromophores of BrC. This is well in agreement with the relatively higher WSOC/OC ratio (avg. $\sim$0.84) during spring. However, the methodology adapted in the present study hinges on the fact that constituents soluble in methanol can be equated with the total organic content. So, the amount of light absorption due to

© 2024 The Author(s). Published by the Royal Society of Chemistry

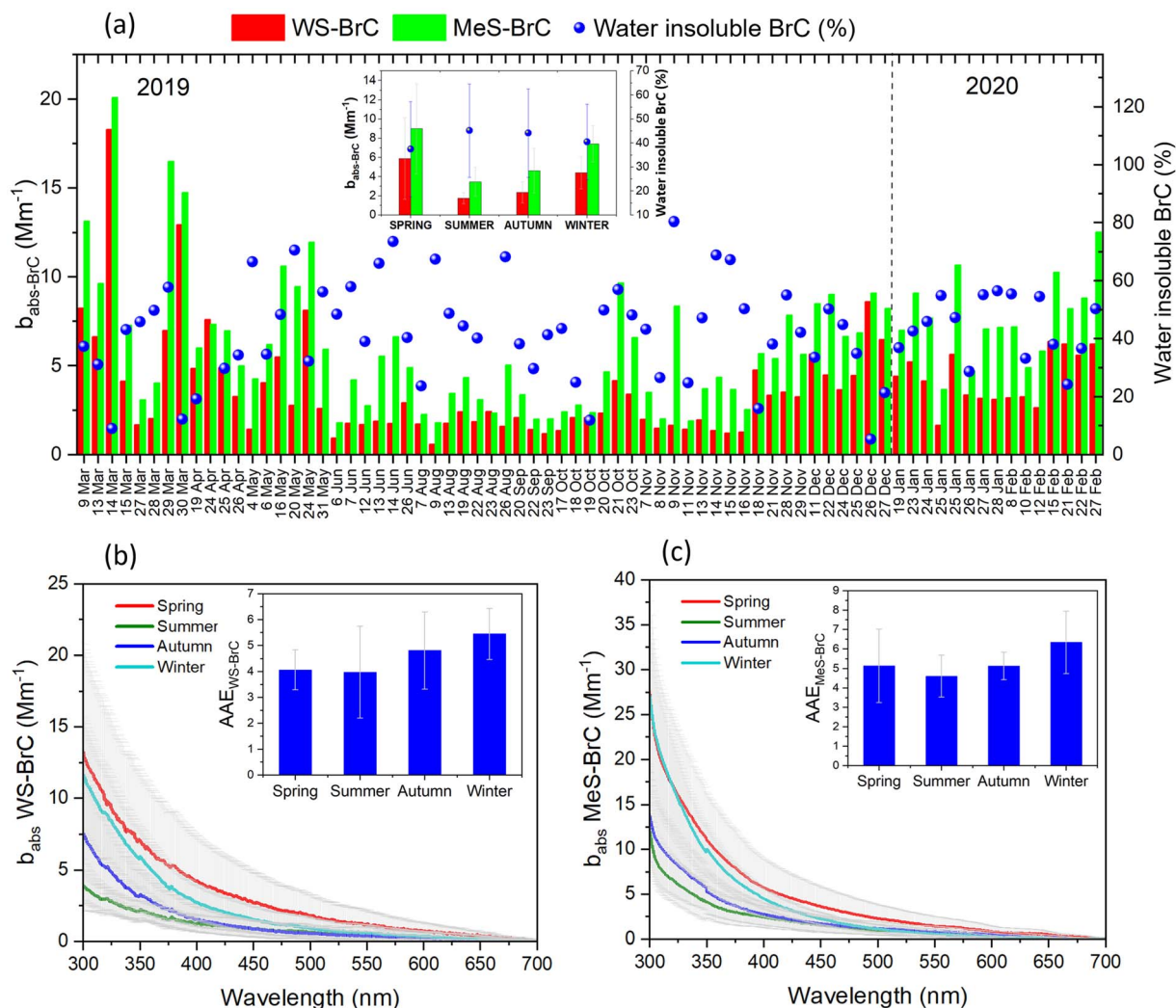*Environ. Sci.: Atmos.*, 2024, **4**, 782–801 | **785**

Fig. 2 (a) Temporal variation of absorption coefficients of WS-BrC and MeS-BrC at 365 nm during the study period at Lachung. Water-insoluble fractions of BrC are given on the right *y*-axis. The seasonal average values are given in the inset. (b) Spectral variation of WS-BrC and its absorption angstrom exponents. (c) Spectral variation of MeS-BrC and its absorption angstrom exponents.

water-soluble components is subtracted from the amount of light absorption owing to methanol-soluble components. This leaves only the absorption due to water-insoluble components, avoiding contributions from components that are soluble in both water and methanol. It is essential to acknowledge here that methanol may not extract all organic constituents[59,60,73] as discussed before. Another factor we need to consider while interpreting this analysis is the potential presence of highly polar organic compounds, which may preferentially dissolve in water rather than methanol. This discrepancy could introduce uncertainties when subtracting the absorption by water-soluble organics from that by methanol-soluble organics. Nonetheless, earlier studies suggest that this highly polar fraction of BrC minimally contributes to BrC light absorption.[19,74] Also, it should be noted here that the methanol-soluble BrC may be significantly lower than the particulate BrC as indicated by earlier studies.[58,75,76] In reality, the insoluble BrC absorption is that obtained from the subtraction from the BrC absorption under ambient (particulate) conditions.[76]

Fig. 2(b) and (c) depict the seasonal changes in spectral variations of the absorption coefficient of WS-BrC and MeS-BrC, respectively, which show a sharp increase in b_{abs} towards shorter wavelengths for both water and methanol extracts. The figure in the inset shows the seasonal overview of the AAE, which illustrates the wavelength dependence of light absorption of BrC over the eastern Himalayas. Within the wavelength range of 300–450 nm, the AAE of WS-BrC in spring, summer monsoon, autumn and winter (4.1, 4.0, 4.8 and 5.5, respectively) is slightly lower than those of MeS-BrC (5.2, 4.6, 5.1 and 6.3, respectively). This spectral variability clearly indicates the additional MeS-soluble chromophores of BrC over Lachung in this wavelength range. The annual average values of the AAE are 4.6 and 5.4 for WS-BrC and MeS-BrC, respectively, indicating a more significant increase in absorption ability from longer to shorter wavelengths. Water-extracted aerosols resulting from incomplete combustion activities usually have an AAE in the range of 1 to 3, whereas those of biomass burning origin displayed an AAE in the range of 6–9.[3,77] Hence, the differences in

786 | *Environ. Sci.: Atmos.*, 2024, **4**, 782–801

© 2024 The Author(s). Published by the Royal Society of Chemistry

Table 1 Comparison of b_{abs}, AÅE and MAE of WS-BrC and MeS-BrC aerosols at Lachung with those at different geographical locations

Region	Site	Period or season	$b_{abs-WS-BrC}$ (Mm^{-1})	$b_{abs-MeS-BrC}$ (Mm^{-1})	AAE_{WS-BrC}	$AAE_{MeS-BrC}$	MAE_{WS-BrC} (m^2 g^{-1})	$MAE_{MeS-BrC}$ (m^2 g^{-1})	References
Himalayas and Tibetan Plateau & other high altitude sites	Lachung	Spring	5.9 ± 4.2	9 ± 4.6	4.1 ± 0.7	5.2 ± 1.8	1.5 ± 0.6	2.1 ± 0.8	Present study
		Summer	1.7 ± 0.5	3.4 ± 1.4	4 ± 1.8	4.6 ± 1.0	1.0 ± 0.3	1.4 ± 0.5	
		Autumn	2.4 ± 1.1	4.6 ± 2.3	4.8 ± 1.5	5.1 ± 0.6	0.79 ± 0.2	1.0 ± 0.4	
		Winter	4.4 ± 1.7	7.4 ± 1.8	5.5 ± 0.9	6.3 ± 1.5	0.75 ± 0.2	0.9 ± 0.2	
		Annual	3.8 ± 2.8	6.4 ± 3.6	4.6 ± 1.4	5.4 ± 1.5	1 ± 0.5	1.3 ± 0.7	
	NCOP	Pre-monsoon	1.83 ± 1.46	2.86 ± 2.49	5.1 ± 0.3	3.9 ± 0.5	0.72 ± 0.15	0.77 ± 0.18	Kirillova et al.[34]
		Monsoon	0.21 ± 0.22	0.32 ± 0.29	4.2 ± 0.6	4.4 ± 1.4	0.45 ± 0.18	0.51 ± 0.15	
		Post-monsoon	0.30	0.72	5.6	3.3	0.36	0.65	
	Lulang	Winter	0.31 ± 0.08	0.61 ± 0.20	5.4 ± 0.6	3.8 ± 0.8	0.61 ± 0.08	0.71 ± 0.13	Zhu et al.[44]
		Winter	1.04 ± 0.25	1.47 ± 0.51	6.7 ± 0.8	8.2 ± 1.4	0.75 ± 0.13	0.71 ± 0.16	
		Pre-monsoon	0.85 ± 0.25	0.97 ± 0.24	6.6 ± 0.6	8.4 ± 0.9	0.62 ± 0.09	0.51 ± 0.12	
		Monsoon	0.38 ± 0.09	0.67 ± 0.17	7.2 ± 0.9	8.1 ± 0.9	0.32 ± 0.07	0.27 ± 0.06	
		Post-monsoon	0.55 ± 0.23	1.09 ± 0.15	7.7 ± 1.3	8.0 ± 1.0	0.44 ± 0.14	0.58 ± 0.05	
	Nam Co	Winter			4.1 ± 1.4		1.2 ± 0.4		Li et al.[119]
	South Eastern Tibetan Plateau	Summer	23.2 ± 11.3		7.22 ± 1.45	5.53 ± 1.04	0.27 ± 0.1	0.34 ± 0.12	Wu et al.[115]
		Winter	11.5 ± 7.79		5.92 ± 0.43	6.24 ± 1.24	0.86 ± 0.17	0.59 ± 0.44	
	Lumbini	Spring	17.0 ± 10.1		3.98 ± 0.39		1.81 ± 0.34		Chen et al.[120]
		Summer	20.4 ± 14.0		4.75 ± 0.60		1.31 ± 0.33		
		Autumn	17.5 ± 12.2		4.37 ± 0.88		1.28 ± 0.21		
		Winter			5.50 ± 0.38		1.41 ± 0.46		
		Annual			4.47 ± 0.74		1.52 ± 0.41		
	Kathmandu valley	Spring			4.8 ± 0.4		1.4 ± 0.2		Chen et al.[99]
		Summer			4.2 ± 0.6		1.0 ± 0.3		
		Autumn			4.9 ± 0.3		1.2 ± 0.2		
		Winter			5.1 ± 0.3		1.5 ± 0.2		
		Annual			4.6 ± 0.8		1.4 ± 0.3		
	Godavari	Winter			5.4 ± 0.4		0.8 ± 0.1		Wu et al.[20]
		Spring			5.2 ± 0.3		1.1 ± 0.2		
		Summer monsoon			5.2 ± 0.7		0.6 ± 0.2		
Urban/semi urban sites	Kochi	2017–2019	16.4 ± 3.41	24.7 ± 3.71	3.68 ± 0.12	3.52 ± 0.31	1.99 ± 0.29	1.94 ± 0.10	Boreddy et al.[72]
	Patiala	Oct. to Dec. 2011	40 ± 18		5.1 ± 1.9		1.3 ± 0.7		Srinivas et al.[62]
	Kanpur	Winter			4.4 ± 0.4		2.5 ± 0.5		Choudhary et al.[116]
	Kharagpur	Nov. to Mar	11 ± 5		6.0 ± 1.1		0.78 ± 0.24		Srinivas and Sarin[17]
	New Delhi	Oct. 2010 to Mar 2011			5.1 ± 2.0		1.6 ± 0.5		Kirillova et al.[117]
	Prayagraj	Spring	8 ± 2.4	11 ± 3			0.92		Alang et al.[68]
		Summer monsoon	3 ± 3.2	3.6 ± 2.4			0.68		
		Post monsoon	22.5 ± 9	29 ± 21			1.34		
		Winter	17 ± 5	18 ± 10			1.27		
	Xian, China	Winter	31.5 ± 16.4		5.2 ± 0.5		1.7 ± 0.2		Choudhary et al.[116]
	Beijing	Winter	15 ± 9.5						Huang et al.[121]
	Nanjing	Spring	4.32 ± 2.28			7.15			Chen et al.[122]
		Summer	3.31 ± 2.36			7.28			
		Fall	4.70 ± 2.35			6.84			

© 2024 The Author(s). Published by the Royal Society of Chemistry

Environ. Sci.: Atmos., 2024, **4**, 782–801 | **787**

Table 1 (*Contd.*)

Region	Site	Period or season	$b_{\text{abs-WS-BrC}}$ (Mm^{-1})	$b_{\text{abs-MeS-BrC}}$ (Mm^{-1})	AAE$_{\text{WS-BrC}}$	AAE$_{\text{MeS-BrC}}$	MAE$_{\text{WS-BrC}}$ (m^2 g^{-1})	MAE$_{\text{MeS-BrC}}$ (m^2 g^{-1})	References
	Seoul, Korea	Winter	9.44 ± 4.70			6.74			Kim et al.[88]
		Spring	3.76	6.56			1.02	0.44	
		Summer	0.87	5.84			0.28	1.45	
		Fall	3.01	6.87			1.02	0.63	
		Winter	7.31	10.93			1.02	0.85	
Oceanic regions	Bay of Bengal, IGP outflow	Nov. 2008	3.6 ± 2.0		5.8 ± 1.5		0.6 ± 0.2		Srinivas and Sarin[79]
		Jan. 2009	2.2 ± 1.3		9.1 ± 2.5		0.4 ± 0.1		
	Indian Ocean, MCOH, Maldives	Feb. to Mar 2012	0.1–0.5		7.2 ± 0.7		0.46 ± 0.18		Bosch et al.[80]

AAE we observed are associated with the diverse composition of organic aerosols over this eastern Himalayan region.

The observed AAE of WS-BrC at Lachung is comparable to the values observed in the background site in the high Himalayas (4.9, 330–500 nm)[34] and New Delhi (5.1, 330–400 nm).[61] The observed values also exhibit a resemblance to that of the water-extracted AAE (5.3, 300 and 450 nm) in aerosols of Xi'an,[58] Guangzhou[78] and Beijing in China.[63] These similarities possibly suggest analogous chemical compositions of BrC chromophores in these regions. Additionally, this resemblance may indicate a degree of consistency in BrC characteristics across these regions. Nevertheless, the AAE at Lachung is significantly lower compared to that reported from the south eastern Tibetan Plateau[44] (365–550 nm range, 6.7 in winter, 6.6 in pre-monsoon, 7.2 in monsoon, and 7.7 in post-monsoon), the IGP outflow to the Bay of Bengal during the winter (9.1, 300–700 nm),[79] the Indian Ocean site on Hanimaadhoo Island during February–March (7.2 ± 0.7, 330–400 nm),[80] the IGP in winter (6.0, 300–700 nm)[17] and winter-spring (6.6)[81] and Beijing (7.18, 310–450 nm).[82] However, very limited information is available for the spectral variabilities of MeS-BrC as compared to WS-BrC (Table 1). The observed values of the AAE of MeS-BrC at Lachung are higher compared to those of the methanol extracts in aerosols from the Nepal Climate Observatory-Pyramid (AAE = 4.0),[34] Los Angeles Basin (4.82, 300–600 nm),[83] and an urban site of Atlanta (4.98, 300–500 nm).[66] However, the AAE values are lower compared to that reported by Soleimanian et al.[84] (8.3 and 8.6 for MeS-BrC and WS-BrC, respectively). In general, the variabilities observed in AAE values across different studies can be ascribed to variations in the composition of extracted chromophores, arising from emission sources and atmospheric processes in distinct study sites.[85] It is important to acknowledge that meaningful comparisons of AAE values are rather hindered by variations in the methodologies used for determining BrC absorption spectrally, as well as discrepancies in the wavelength bands reported across different studies.

The estimated AAE values in this study are relatively elevated during the winter (5.5 for WS-BrC and 6.3 for MeS-BrC). This phenomenon can be attributed to escalated wood burning activities prevalent during colder months, particularly for heating purposes. It is noteworthy that earlier studies in diverse geographical regions have highlighted the impact of wood burning on the spectral absorption characteristics of BrC aerosols.[60,76,77] Paraskevopoulou et al.[66] for instance, documented substantially higher AAE values for WS-BrC during winter (8.3) in Europe, a region where residential wood burning activities exert a pronounced influence, surpassing those observed in our study over the eastern Himalayas. The higher AAE values of 7.2 and 7.6 for WS-BrC during winter were reported in Beijing[63] and Los Angeles.[83] The lower AAE during summer indicated the photobleaching of secondary organic compounds, which would absorb at higher wavelengths.[86] Moreover, studies have shown that the colder periods are highly influenced by the contributions of polycyclic aromatic hydrocarbons (PAHs) compared to the warmer months.[84] High-molecular-weight (HMW) PAHs have the ability to contribute more to the total particle-phase PAHs during the warmer season

due to the higher ambient temperatures, which encourage the partition of low-molecular-weight (LMW) PAHs to the gas-phase. There are both LMW and HMW particle-phase PAHs present during the cold period due to the lower ambient temperatures that promote the gas-to-particle conversion of LMW PAHs.[87] During the warm period, PAHs predominantly absorb radiation from longer wavelengths of the visible spectrum due to the absence of LMW PAHs, which typically absorb shorter wavelengths.[73,83] This leads to an increase in the AAE of MeS-BrC from the summer to winter period. The similar seasonality in the AAE of MeS-BrC exhibiting higher values during winter compared to summer is observed in earlier studies in distinct environments.[84,88]

The seasonal variability in the AAE of MeS-BrC at Lachung in our study exhibited a distinct pattern compared to that of WS-BrC, with the AAE of MeS-BrC during spring (5.2 ± 1.8) slightly exceeding that during summer and autumn. This observation implies a heterogeneous nature of MeS-BrC chromophores. The elevation in MeS-BrC AAE during spring might be associated with the formation of stable secondary non-polar chromophores, which are comparatively more resilient during long-range atmospheric transport.[89] This observation aligns with the findings reported by Paraskevopoulou et al.,[60] who observed an enhanced AAE of MeS-BrC due to photobleaching of BrC aerosols. The mean AAE of WS-BrC at Lachung was comparatively lower than those observed for MeS-BrC. This difference can potentially be attributed to the lower influence of HMW chromophores, which are typically generated by biomass burning, within the MeS-BrC fraction. These chromophores possess the capacity to absorb light within the visible portion of the electromagnetic spectrum. Interestingly, this finding is in contrast with the observations by Paraskevopoulou et al.,[60] wherein they found a decrease in the AAE values for MeS-BrC during winter. This decrease was attributed to the strong presence of HMW chromophores resulting from residential wood burning during the colder months.[60] Several other studies also corroborated the lower AAE of MeS-BrC.[34,58,66,82–84] They have also attributed the higher absorption for MeS-BrC above 400 nm to the presence of HMW chromophores, which are solely extractable in methanol. Since less-polar chromophores are extracted mostly in methanol than water, and absorb more light at higher wavelengths, Zeng et al.[89] found a lower AAE for MeS-BrC compared to WS-BrC in the smoke plumes. Similar to our observations, the higher values of AAE of MeS-BrC were also reported by Zhu et al.[44] in the south eastern Tibetan Plateau region (AAE = 8.2 for MeS-BrC and AAE = 6.9 for WS-BrC).

Less or non-polar chromophores are more likely to dissolve in methanol compared to water. These chromophores typically have fewer polar functional groups and are more hydrophobic in nature, whereas highly polar chromophores contain more polar functional groups and are more hydrophilic.[3,90] In the context of higher extraction of macromolecules, particularly HMW hydrocarbons (HCs), in methanol compared to water in the near-visible spectrum, nonpolar compounds, including higher-weight hydrocarbons, tend to aggregate and interact via hydrophobic interactions in aqueous environments.[3,4] This can reduce their solubility and extraction efficiency in water. In contrast, methanol provides a less polar environment, reducing the propensity for hydrophobic interactions and promoting better solubility and extraction of hydrophobic macromolecules. Macromolecules such as HMW HCs often exhibit absorption in this range due to their complex molecular structures and electronic transitions.[3,4,90] Methanol, being a transparent solvent allows for better detection and characterization of these absorption features compared to water, which absorbs more strongly in the near-visible spectrum due to its higher polarizability.[3] HMW chromophores typically absorb more light at longer wavelengths, leading to lower AAEs. Due to their reduced solubility compared to smaller molecules, insoluble species of these chromophores may not be fully captured during extraction. This can occur since particles with chromophores insoluble in water but potentially soluble in methanol might be missed during initial water extraction and subsequently removed by the liquid syringe filter, excluding them from measurement. Additionally, there could be particles which are fundamentally insoluble in methanol and therefore unidentified during extraction.

The highest values of b_{abs365} observed during spring and winter for both WS-BrC and MeS-BrC are comparable with the temporal evolution of WSOC and OC concentrations (Fig. 3). During the study period, OC concertation ranged from 1.6 to 14.7 µg m^{-3}, showing about 9-fold variation, while WSOC varied from 0.85 to 8.2 µg m^{-3}. We found a consistent correlation (>0.6) between the concentrations of OC and WSOC suggesting their similar physical processes, encompassing both similar production and transport. The relatively higher contribution of water-insoluble BrC observed during summer is associated with the relatively higher fraction of WIOC (>30%) with the carbonaceous aerosols during this period.

The higher association (Fig. 4) between the concentrations of WSOC and WS-BrC light absorption coefficient at 365 nm (b_{abs365}) revealed that the sources of the WSOC fraction of aerosols strongly influence the ability of WS-BrC aerosols to absorb light. Likewise, the MeS-BrC light absorption coefficient at 365 nm (b_{abs365}) shows an impressive association with OC concentrations. This shows that the MeS-BrC light absorption properties are significantly influenced by the OC content. The higher b_{abs} values for MeS-BrC, measured at shorter wavelengths, can be primarily attributed to the higher amount of extracted organic matter in methanol. The stronger correlations imply that BrC chromophores, which absorb at 365 nm, make up an important part of WSOC or OC.

The measured aerosol light absorption (b_{abs365}) in the vicinity of Lachung surpasses previous findings in the HTP region.[34,44] This difference is potentially linked to the predominant influence of light-absorbing BrC chromophores prevalent in the eastern Himalayan region, facilitated by long-range atmospheric transport. Moreover, the b_{abs365} recorded at Lachung exhibits a lower magnitude compared to observations conducted in urban and oceanic regions across South Asia.[62,65,68,72] Furthermore, our findings indicate a lower b_{abs365} in contrast to measurements obtained during warmer and colder periods in other studies. For example, Soleimanian et al.[84] reported b_{abs365} values of 3.7 Mm^{-1} for WS-BrC and 10.1

© 2024 The Author(s). Published by the Royal Society of Chemistry

Environ. Sci.: Atmos., 2024, **4**, 782–801 | **789**

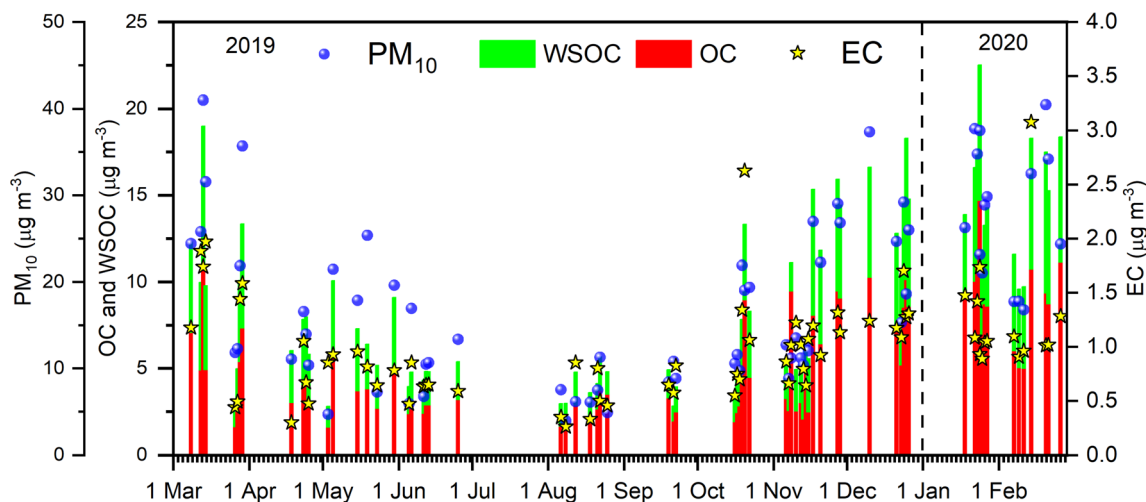**Fig. 3** Temporal variations of PM_{10}, OC, WSOC and EC at Lachung during the study period.

Mm^{-1} for MeS-BrC during warm and cold seasons, respectively. Additionally, Cheng et al.[114] documented a b_{abs365} value of ~26 Mm^{-1} during the cold season in Beijing. These discrepancies can be attributed to the variations in chemical composition of BrC chromophores originating from diverse sources.

Several studies pointed out higher light absorption by MeS-BrC than WS-BrC. For example, Soleimanian et al.[84] found that MeS-BrC absorbs light 3.7 times more than WS-BrC. Zhang et al.[83] found ~5 times higher absorption of MeS-BrC compared to WS-BrC. Compared to these observations, we observed the lowest ratio of MeS-BrC to WS-BrC at Lachung, since the water-soluble organics dominated throughout the year. We observed an increasing trend in the water-insoluble to water-soluble BrC fraction during the summer followed by autumn, which further corroborates the higher levels of water-insoluble organic aerosols during the warmer period as compared to winter. Our observations differ from the observations by Soleimanian et al.[84] in central Los Angeles, where they found high levels of water-insoluble BrC during the colder periods of the year. Soleimanian et al.[84] found that fossil fuel emissions were the main source of BrC light absorption during the warmer months at central Los Angeles. On the other hand, biomass burning from domestic activities was the main source during the cooler months.

The effect of aged biomass burning derived aerosols is notable in spring at Lachung, while in summer, the fraction of biogenic aerosols and the relative dominance of fossil-fuel combustions are higher, which resulted in less solubility and higher fractions of water-insoluble aerosols. We found high OC concentrations during winter, whereas the b_{abs} is higher during spring. This indicated that the organic aerosols at Lachung during winter contain less light absorptive BrC chromophores compared to the spring season. In our previous study,[52] we found biomass burning to be the dominant source of organic aerosols at Lachung with a significant contribution from residential combustion emissions during winter. We found a higher OC/EC ratio together with a higher WSOC/OC ratio at Lachung during all seasons with higher relative contributions

during spring and winter. Kaskoutis et al.[91] found WS-BrC from fast oxidation processes in winter, whereas the absence of local biomass burning sources in summer, combined with photochemical processing and aging of regional organic aerosols resulted in higher WSOC/OC fractions. The ratios of WSOC to OC are influenced by both primary organic emissions and secondary atmospheric processes, as highlighted by Rai et al.[92] Furthermore, the studies suggested that the fresh wood burning sources are highly water-soluble in nature.[84] The increased solubility of biomass burning aerosols could potentially amplify aerosol–cloud interactions and contribute to the formation of haze/fog.[93] According to Srinivas and Sarin,[79] there was a marked decline in BrC absorption from the IGP to the receptor oceanic region across the Bay of Bengal. This is because the contribution of non-absorbing WSOC and/or photo-bleaching of BrC during long-range atmospheric transport was increased relative to the other factors.

The higher ratios of WSOC/OC at Lachung in all seasons of the year suggest the dominance of secondary organic aerosols at this remote high-altitude site.[52] We observed a significant correlation of b_{abs} of WS-BrC and Mes-BrC with NH_4^+, SO_4^{2-}, $C_2O_4^{2-}$ and methane sulfonate (MSA) during spring. MSA indicates biogenic sources whereas $C_2O_4^{2-}$ is generally used as a tracer for SOA generated by aqueous-phase processes because its direct emissions are probably negligible.[94] We have identified earlier[52] that the aqueous phase formation of organic aerosols at Lachung during spring is associated with different biogenic and anthropogenic sources. This suggests the enhanced BrC formation at Lachung through aqueous-phase formation mechanisms during long-range atmospheric transport. Additionally, the correlation between b_{abs} and K^+ is strong during spring (Fig. 4), indicating the influence of biomass burning derived organic aerosols on BrC absorption at Lachung.

This result is further supported by the higher biomass burning activities during spring (Fig. 5). Earlier studies[4,95,96] showed that the optical characteristics of BrC are influenced by
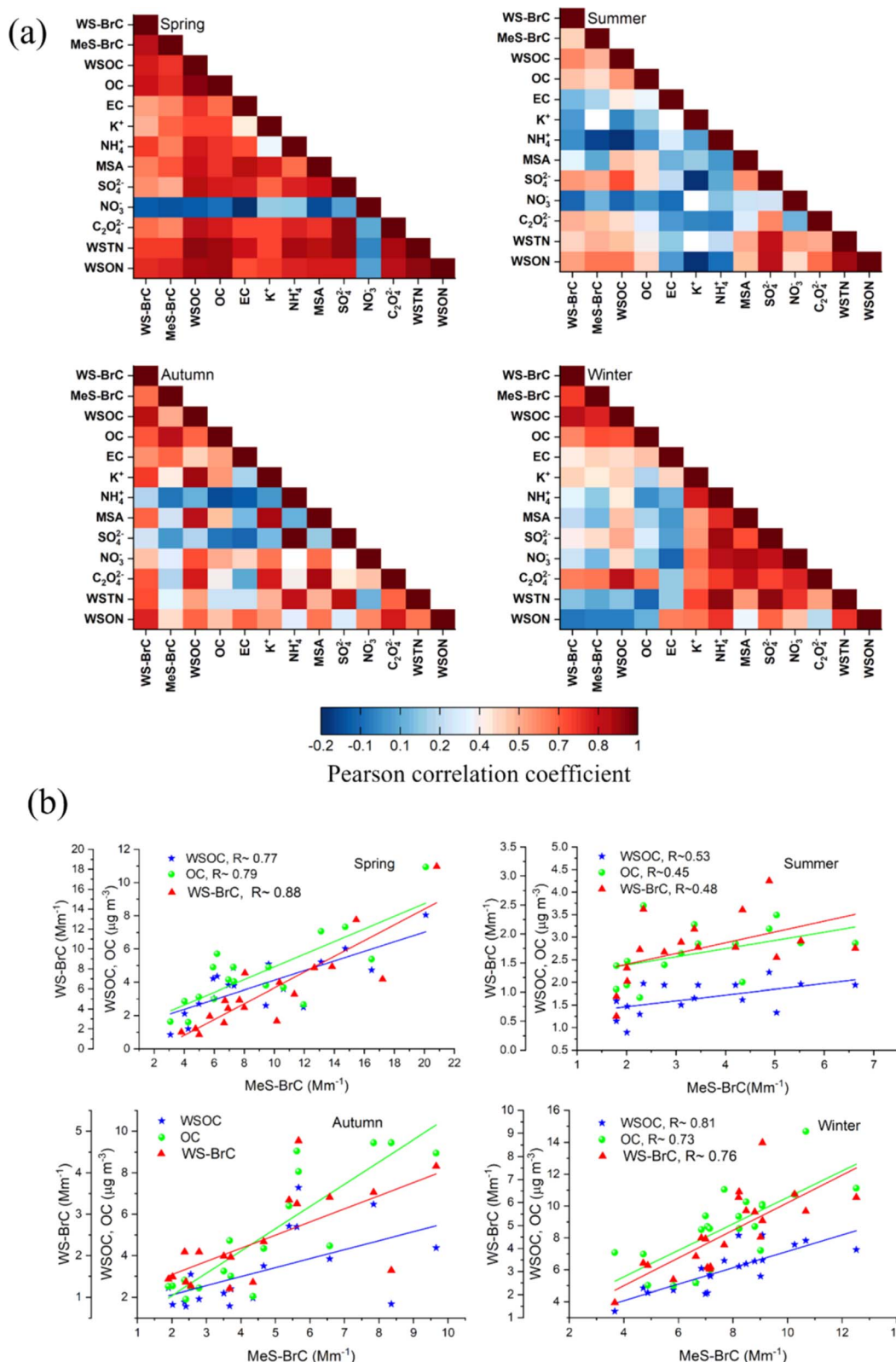
Fig. 4 (a) Pearson correlation between the different chemical components, (b) Pearson correlation of MeS-BrC with WSOC, OC and WS-BrC during distinct seasons.

different types of biomasses, burning conditions as well as their atmospheric aging processes. In addition, in spring, we observed good correlations of WSTN and WSON with the

absorption coefficient of BrC for water and methanol extracts. This suggests the influence of various nitrogenous compounds in the BrC aerosols during spring. This was further
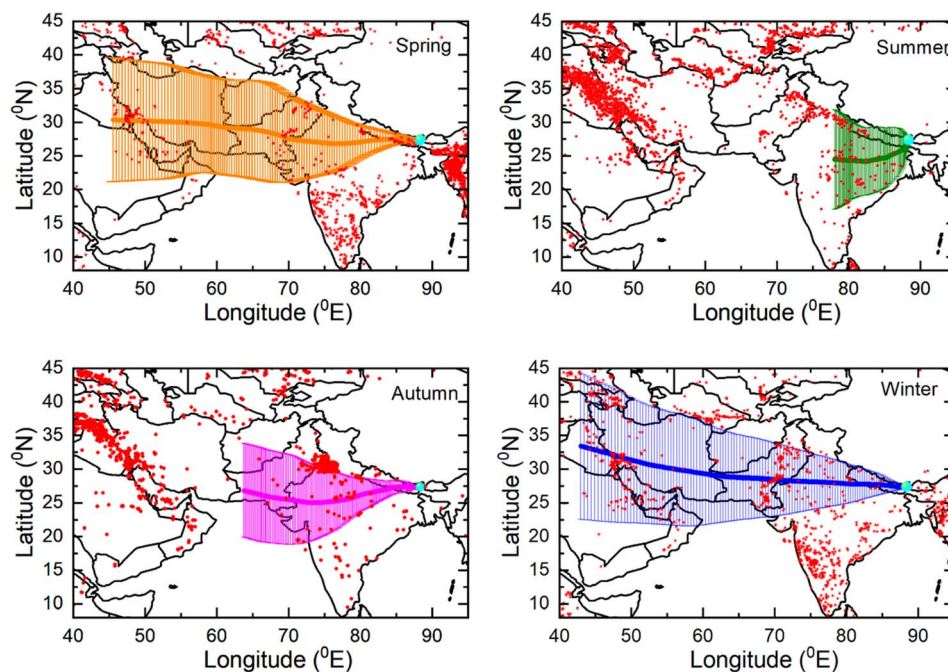
© 2024 The Author(s). Published by the Royal Society of Chemistry

Environ. Sci.: Atmos., 2024, 4, 782–801 | 791

Fig. 5 7 day HYSPLIT airmass back trajectories arriving at 500 m above the ground level at the observational site during different seasons. The fire count values obtained from using SUOMI VIIRS C2 data (last access: 10th December 2023) are shown in the background.

corroborated by a relatively high WSON/WSOC ratio (0.27) during this period compared to other seasons, which indicates the presence of a more significant portion of water-soluble nitrogenous organic compounds as compared to water soluble organic carbon. Satish and Rastogi[19] highlighted the significance of nitrogenous compounds in BrC produced through secondary organic aerosols in the presence of a high level of NOx due to biomass burning. It should also be noted that the absorption characteristics of BrC generated by emissions from burning biomass sources can be governed by nitrogen containing organic compounds in the atmosphere.[97,98]

Furthermore, we observed significant correlation between WS-BrC species and WSTN (R ~0.7) and WSON (R ~ 0.8), suggesting the presence of water-soluble nitrogen BrC chromophores during autumn. This could be possibly associated with the influence of post-agricultural burning processes during this period. Also, the correlation between b_{abs} and K^+ is higher (R ~ 0.8), during this period indicating the influence of biomass burning sources on BrC absorption at Lachung. During autumn, there is a correlation of WS-BrC with K^+ (R ~ 0.75), MSA (R ~ 0.68), $C_2O_4^{2-}$ (R ~ 0.7), and NO_3^- (R ~ 0.5), whereas the association of these components with MeS-BrC is less significant. This suggests the water-soluble chromophores of BrC aerosols are mainly driven by the sources of K^+, MSA, $C_2O_4^{2-}$ and NO_3^-. This along with the higher association of WS-BrC with K^+ and NO_3^-, further supports our inference of the influence of the post-agricultural burning process and biogenic sources on modulating the WS-BrC over Lachung during autumn.

Biomass burning is a prime source of organic aerosols, including water-soluble BrC and methanol-soluble BrC. In

spring, a notable correlation (R ~ 0.53) between WS-BrC and a tracer of biomass burning (K^+) is evident, whereas the correlation is very poor in summer (R ~ 0.03), indicating the biomass burning influence on the WS-BrC during spring at Lachung in the eastern Himalayas. These findings underscore the seasonal variability in aerosol composition and sources at Lachung. Since biomass burning activities typically decrease in summer due to reduced agricultural burning or forest fires and increased precipitation due to the summer monsoon, the observed weakening of the correlation of WS-BrC with K^+ aligns with seasonal patterns in the influence of biomass burning emissions at Lachung.

Regional emission sources such as domestic burning activities are responsible for the higher concentrations of PM_{10} and associated carbonaceous species at Lachung during winter. The influence of the lower boundary layer might have also resulted in the elevated loading of PM_{10} and carbonaceous species during winter. The significant positive relationships of b_{abs} of WS-BrC and MeS-BrC with K^+ confirms the biomass burning-derived organic aerosols modulating the absorption of BrC during this period. During the summer monsoon period, we observed a good association of BrC with SO_4^{2-} and $C_2O_4^{2-}$, suggesting a strong relationship of BrC with organic aerosols produced *via* photochemical oxidation processes. Moreover, there were significant correlations between WS-BrC and WSTN (R ~ 0.47) and WSON (R ~ 0.57), as well as MeS-BrC and WSTN (R ~ 0.54) and WSON (R ~ 0.67), indicating that nitrogenous chromophores had an impact on BrC absorption during this period.

We would like to point out here that the absolute concentrations of OC and WSOC at Lachung are relatively higher

during winter than spring, whereas the higher absorption contribution by BrC is higher during spring than winter. Notably, the spring time enhancement in the absorption by BrC is modulated by more significant atmospheric processing of biomass burning-derived organic aerosols *via* long range atmospheric transport. We infer that more atmospherically processed organic aerosols in spring perhaps contain more light absorbing BrC chromophores than those in winter where the organic aerosols were mostly of local origin due to the lower boundary layer. Higher concentrations of PM_{10} and the associated carbonaceous species at Lachung during winter could be attributed to the regional emission sources during winter, specifically due to the burning activities such as wood burning, cookstove emissions, *etc.* due to colder days in this season. During winter, the correlation of WS-BrC and MeS-BrC with sulfate and oxalate showed almost similar correlations. This is also indicative of the role of secondary formation of BrC in the aqueous phase during this period with higher relative humidity.[72]

A strong correlation was observed between WS-BrC and MeS-BrC absorptions in spring (R ~ 0.88, slope ~0.97), indicating their common sources.[60,99] This relationship is reduced to about half in summer (R ~ 0.48, slope ~1.3), when there is substantial heterogeneity regarding the origin, lifetime and fate of different BrC chromophores.[84,85] During spring and autumn, we observed a strong correlation between b_{abs} of WS-BrC and MeS-BrC and EC, suggesting the common emission sources of BrC and EC. However, the weak correlation during summer indicates the large heterogeneity in EC and BrC sources. The lower correlations of BrC with EC and K^+ indicated that the BrC absorption was less related to primarily derived biomass burning aerosols during this period.

During autumn, we observed a significant correlation of WS-BrC with nitrate (R ~ 0.5) and $C_2O_4^{2-}$ (R ~ 0.7), indicating the secondary formation of water-soluble compounds like nitrated aromatics.[100] A comparable correlation was also reported between WS-BrC and nitrate during the biomass burning episode in the IGP[76] and Europe.[60] During autumn, the IGP regions are significantly influenced by the intense biomass burning emissions due to the post-harvest burning activities. Similarly, this is also possible at Lachung since the post-agricultural burning activities are intense during this period in the eastern part of India. This would have significantly contributed to the sources of BrC during this period. This is also supported with the higher correlation of BrC with K^+. Under biomass burning conditions, the formation of secondary WS-BrC was also reported in earlier studies.[101]

For lower values of OC during autumn (OC < 4.5 μg m^{-3}) (Fig. 4b), we observed a higher correlation between WS-BrC and MeS-BrC, which also means the MeS-BrC increases at a lower rate in this case. Whereas for overall OC, the MeS-BrC increases at a higher rate with WS-BrC. In this case, the correlation of MeS-BrC with WSOC, WS-BrC and K^+ increased to R ~ 0.5, R ~ 0.6 and R ~ 0.45, respectively. However, the correlation of MeS-BrC with EC and NOx reduced significantly (R ~ 0.06 and R ~ 0.01). This suggested that the lower values of OC during autumn are associated with secondary organics from biomass

emissions, whereas the higher values are more associated with the primary emissions together with EC. This inference was also supported by the apparent increase in the correlation of MeS-BrC with sulfate and oxalate. MeS-BrC showed a weaker association with WSOC and OC during summer, which decreased considerably for higher values of OC and WSOC. Sarkar *et al.*[102] and Satish *et al.*[103] found that the summertime lower correlation of WS-BrC and MeS-BrC is associated with several factors such as the recirculation of aged aerosol, formation of non-absorbing SOA and BrC photo-bleaching. During summer when the OC values are <3 μg m^{-3}, we observed a significant increase in the correlation of MeS-BrC with WS-BrC (0.62), OC (0.62), SO_4^{2-} (0.76) and oxalate (0.6). This suggested strong photo-chemical oxidation processes during summer. Furthermore, the increase in correlation of MeS-BrC with OC suggested more contribution by insoluble BrC to MeS-BrC absorption during this period. Similar observations were not found during the other seasons.

The observed variability in light absorption by BrC is a complex phenomenon influenced by various factors such as sources, including the burning of crops, wood, and fossil fuels, the processing of organic aerosols during long-range transport through the atmosphere, and the prevailing meteorological conditions over the Himalayas. Fig. 5 shows the 7 days seasonal HYSPLIT[104] airmass back-trajectories arriving at the observational site at 500 m above the ground level. The composition of aerosols at Lachung during spring is mostly associated with the long-range atmospheric transport of north westerly airmasses associated with higher fire activities, indicating the abundant influence of biomass burning during this period. This significantly influences the observed absorption enhancement by BrC in this high-altitude region during spring.

Bonasoni *et al.*[105,106] found that the passage of an atmospheric brown cloud has a significant impact that is attributed to several parameters in the Himalayas during the spring season. These parameters include the maximum seasonal mixing layer height, increased emissions largely from biomass burning of agricultural waste, and substantial up-valley winds along the Indo-Gangetic Plain and the Himalayan foothills. However, it should be noted that the wind regime across the Himalayas undergoes changes during the summer monsoon, with the prevailing winds shifting to the south, leading to a decline in wind patterns.[106] The summer monsoon also brings about a vital atmospheric process known as wet scavenging, whereby rainwater effectively removes pollutants. This process plays a crucial role in lowering the aerosol concentration levels in South Asia during the summer monsoon. The significance of efficient wet scavenging in reducing pollution levels has been highlighted in studies conducted by Kirillova *et al.*[107] Our observations showed a significant contribution of light absorption by BrC from the IGP regions specifically during spring and summer monsoon. Similar to our observations, Zhu *et al.*[108] identified the major potential sources of BrC in the HTP region where the IGP, the north western Chinese regions, and the interior of the TP were identified as the major sources. In addition, our observations of the contribution by biogenic and anthropogenic sources at Lachung in light absorption,

© 2024 The Author(s). Published by the Royal Society of Chemistry

Environ. Sci.: Atmos., 2024, **4**, 782–801 | 793

especially during spring and autumn, support the observations by Wang *et al.*[109] where they demonstrated the impact of biogenic emissions from broad-leaved and pine trees, as well as the local anthropogenic emission contribution to the formation of secondary BrC in the HTP region. They have also proposed the photooxidation of natural biogenic precursors, including isoprene, α-pinene, and limonene, as a potentially significant pathway for secondary BrC formation over the high altitudes of the HTP.

3.2 Mass absorption efficiency of BrC

Mass absorption efficiency (MAE) is a crucial absorption characteristic of aerosols that determines the connection between its atmospheric abundance and radiative forcing. MAE reflects the mass normalized light absorption efficiency of BrC chromophores, which is determined mainly by the chemical structure of the chromophores, including their molecular weight, degree of unsaturation and oxidation state, as well as the proportion of chromophore species to organics that do not absorb light. We determined wavelength-dependent MAE values of BrC in PM_{10} aerosols of Lachung for the campaign period. The seasonal changes in the MAE values at 365 nm (MAE_{365}) for WS-BrC and MeS-BrC in aerosols at Lachung are presented in Fig. 6.

Similar to b_{abs365}, MAE_{365} of MeS-BrC is also relatively higher than those of WS-BrC during the campaign, signifying that organic aerosol extracted in methanol possesses greater light-absorbing potential per unit mass at shorter-wavelength than water-soluble organic carbon. We found high MAE_{365} of WS-BrC (1.5 ± 0.6 m^2 g^{-1}) and MeS-BrC (2.07 ± 0.8 m^2 g^{-1}) during springtime, whereas the values are substantially lower during the winter period (WS-BrC: 0.75 ± 0.16 m^2 g^{-1} and MeS-BrC: 0.9 ± 0.21 m^2 g^{-1}). The high MAE_{365} in springtime aerosols infers more efficient absorption of UV-visible light compared to aerosols of other seasons. This is possibly due to the fact that organic aerosols in spring have biomass-burning origin and endured atmospheric photochemical processing in the aqueous phase. This result is further evidenced by the backward trajectories of air masses and fire activities in the south Asian region

displayed in Fig. 5. The higher range of MAE values in spring suggest lower homogeneity in sources and the effect of long-range transported air masses with different characteristics. Reversely, the small MAE range in winter shows the local influence and more standard conditions regarding the light-absorbing carbonaceous aerosols.

It was observed that the production of high-molecular-weight chromophores or oligomers in the atmosphere due to aqueous phase photochemical reactions is accountable for the enhancement in absorbance of BrC aerosols.[110,111] Furthermore, biomass burning derived aerosols contain considerable levels of aromatic compounds such as organic acids, carbonyls, and phenols,[98] which form oligomers by radical coupling reactions involving either an oxygen atom of the hydroxyl functional group or a carbon atom of the aromatic ring during aqueous phase photooxidation processes.[112,113] Notably, these compounds can potentially enhance the light absorption of BrC aerosols. During winter, more localized burning events and the lower boundary layer height might have impacted the characteristics of BrC aerosols at Lachung. The lowest MAE_{365} values of WS-BrC and MeS-BrC during winter are associated with high OC concentrations. It should be noted here that, as discussed in the previous sections, the attribution of entire OC values to MeS-BrC can bias the MAE values. Although considerable variability observed in the MAE values of BrC can be attributed to several factors, we presume that substantial seasonal changes in MAE_{365} in BrC aerosol at Lachung might be influenced not only by its absorption efficiency but also by the OC and WSOC concentrations, as well as the size distribution of aerosol particles over the eastern Himalayas. Cheng *et al.*[114] reported that fine particles with a lower mass median aerodynamic diameter contribute to higher MAE. We observed a higher fraction of fine particles in our earlier studies at Lachung during spring.[51] The greater MAE of WS-BrC and MeS-BrC aerosols, and the higher proportion of OC (25–32%)[52] at the observational site highlights a crucial role of BrC aerosols in inducing the atmospheric radiative forcing in the elevated region of the Himalayas. Another possible explanation is that different BrC species exhibit distinct absorption properties. Moreover, their relative abundances may also vary under different meteorological conditions. Additionally, specific meteorological conditions have the potential to either decrease or enhance the absorption properties of BrC chromophores.[3,4] These chromophores may originate from both primary and secondary BrC species, which are emitted from anthropogenic sources such as biomass burning and fossil fuel emission sources, and they can possess diverse absorption characteristics.

The MAE_{365} of WS-BrC during winter in aerosol samples at Lachung is comparable with the MAE_{365} estimated at NCO-P Station (PM_{10}: 0.61–0.71 m^2 g^{-1}),[34] the IGP ($PM_{2.5}$: 0.78 m^2 g^{-1}),[17,68] over the Indian Ocean sector (TSP: 0.6 m^2 g^{-1}),[79] East Asian outflow at the Gosan site in the Jeju Island ($PM_{2.5}$ and TSP: 0.65–0.75 m^2 g^{-1}),[61] and Seoul.[88] Moreover, MAE_{365} obtained in the present study is higher compared to the MAE_{365} estimated from low-altitude stations in remote areas[20,115] and the Indian Ocean (PM_{10}: 0.4 m^2 g^{-1}, $PM_{2.5}$: 0.46 m^2 g^{-1}),[79,80] but lower than that from other urban sites in South Asia during
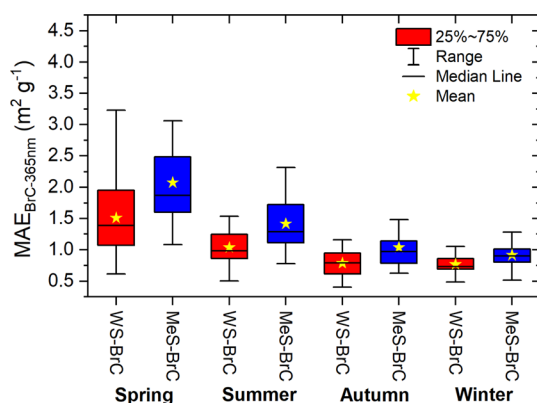

Fig. 6 Seasonal mass absorption efficiency (MAE) of WS-BrC and MeS-BrC at 365 nm in aerosols of Lachung in the eastern Himalayas.

winter.[72,116] The comparison of the MAE_{365} of wintertime aerosols with the continental urban locations suggests lower absorption due to BrC aerosols under the remote background conditions. MAE_{365} of WS-BrC and MeS-BrC at Lachung during spring, which is associated mainly with long-range transport and the aqueous phase processing of organic aerosols, is comparable to those in the pollution source regions of the IGP such as the megacity New Delhi ($PM_{2.5}$: 1.6 m^2 g^{-1})[117] and Patiala ($PM_{2.5}$: 1.3 m^2 g^{-1}).[62] Wang *et al.*[109] reported high absorption by BrC in the south eastern part of the Tibetan Plateau due to the long-range atmospheric transport of biomass burning-derived organic aerosols. Likewise, Shen *et al.*[118] reported higher absorption due to the aqueous phase production of BrC at an urban site in China. More comparison between the observed absorption properties of BrC aerosols at Lachung with other high or lower altitude and continental or oceanic regions is provided in Table 1. Based on these comparisons, it can be inferred that the study region exhibits higher abundances and greater absorbing capacity of BrC chromophores, similar to what has been reported in continental lower elevated regions of South Asia. These data show that BrC tends to have higher MAE_{365} in association with substantial anthropogenic influence. Moreover, we found that the characteristics of BrC aerosols at Lachung are similar to those reported in the Indian Ocean and the Bay of Bengal as reported by Bikkina and Sarin.[65] However, the AAE at Lachung is different from that observed in other regions. This demonstrates that the Lachung site exhibits stronger WSOC or OC absorption at longer wavelengths than the remote oceanic regions largely affected by South Asian pollution outflow.

3.3 Imaginary refractive index of WS-BrC and MeS-BrC aerosols

The imaginary refractive index of BrC (k) indicates the absorption ability of the BrC aerosols. Fig. 7 shows the estimated values of the imaginary refractive index as described in Section 2.2. The estimated k values of WS-BrC (MeS-BrC) were higher during spring (0.06 ± 0.02 and 0.09 ± 0.03) associated with the atmospheric processing of aerosols and with the long-range

atmospheric transport of biomass burning aerosols during this period, as discussed before. Interestingly, lower values of k were found during winter (0.032 ± 0.007 for WS-BrC and 0.04 ± 0.01 for MeS-BrC). The lower k values during winter show the reduction in absorption by BrC aerosols due to the photobleaching during this period. These lower values of k were comparatively lower than the k values reported from Patiala ($k_{\text{WS-BrC}}$ of 0.061 ± 0.034, a region that is heavily influenced by the primary biomass burning in the IGP).[18] The lower k values observed at Lachung clearly show the reduction in absorption by the photochemically aged aerosols at this site. This suggests that even though the aerosols at Lachung during winter are impacted mostly by burning activities, various atmospheric factors and the chemical processing of aerosols at Lachung modulate the absorption ability of BrC aerosols over at this remote region.

Laboratory-based investigations have provided insights into the light absorption characteristics of BrC aerosols and their correlations with EC/OM ratios estimated for different combustion sources.[123,124] Saleh *et al.*[97,123] suggested that the extent of absorption is primarily governed by the combustion conditions rather than the type of fuels. Furthermore, Saleh *et al.*,[97] proposed a linear relationship between k and the BC/OA ratio for a wide range of biofuels in climate models. This relationship is crucial in accounting for regionally varying radiative forcing caused by BrC aerosols. Consequently, we have examined the interconnections between the optical properties of BrC and their associations with the ratio of EC/OM in aerosols at Lachung (Fig. 8). No apparent linear correlation between k and EC/OM is observed in the present study in the eastern Himalayas. This absence of a linear relationship underscores the need to harmonize the present parametrization of BrC optical properties derived from real ambient aerosols with those obtained from controlled chamber experiments. Similar observations were also documented by Bikkina and Sarin,[65] and Shamjad *et al.*[125] in the south Asian region. Bikkina and Sarin[65] examined the correlation between k of WS-BrC and the EC/OM ratio in aerosols collected over the Indian Ocean, taking into account the impact of crop residue burning and wood burning on the IGP. They also did not find a linear correlation between k
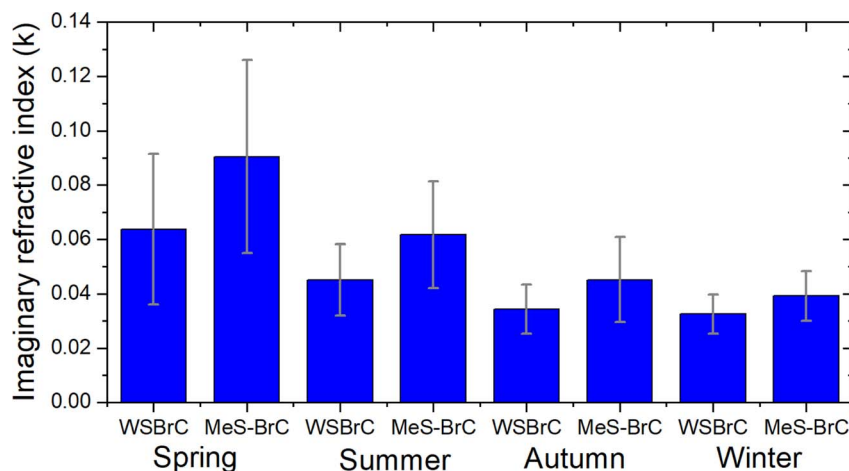

Fig. 7 Seasonal imaginary refractive index of water-soluble BrC ($k_{\text{WS-BrC}}$) and methanol-soluble BrC ($k_{\text{MeS-BrC}}$) during the campaign period.

© 2024 The Author(s). Published by the Royal Society of Chemistry

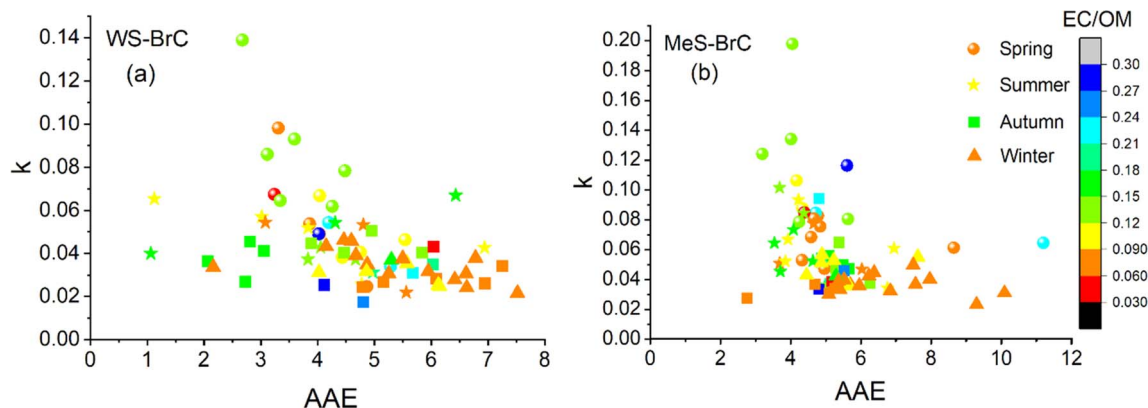*Environ. Sci.: Atmos.*, 2024, **4**, 782–801 | **795**

Fig. 8 (a) Imaginary refractive index (k) of WS-BrC as a function of absorption angstrom exponent (AAE) for various EC/OM ratios during the study period, (b) k of MeS-BrC as a function of AAE for various EC/OM ratios during the study period.

and EC/OM. However, they found that k of WSOC and AAE was inversely related in the IGP outflow and suggested that there were other atmospheric processes besides fuel type and combustion conditions, which affect BrC absorption characteristics such as photobleaching and organic matter oxidation during long-range transport. At an urban site in the IGP, Shamjad et al.[125] found that WSOC mostly absorbs light within a limited wavelength range of 365–470 nm, while OC absorbs light across a broader wavelength range (365–565 nm). Therefore, the total absorption of OC depends on the proportionate presence and absorptive characteristics of WSOC. In our study, we observed a notable inverse linear correlation of k with the AAE of WS-BrC and MeS-BrC aerosols (Fig. 8). Notably, this relationship was more pronounced in the WS-BrC aerosols during the spring (R ~ −0.8). This enhanced correlation can be attributed to the oxidation of organic matter during long-range atmospheric transport. Furthermore, Choudhary et al.[116] examined the variations in k of WS-BrC at a wavelength of 365 nm with respect to that of the AAE at different locations in the South Asian region during the winter season. They found a robust association (R ~ 0.92) between k of WS-BrC-365 and AAE, consistent with the findings of Saleh et al.[97] in the south Asian outflow. Conversely, a less pronounced correlation (R ~ 0.53) was observed in the atmosphere over the Himalayan region. The observations by Choudhary et al.[116] indicated that photo-bleaching plays a more significant role than dilution in controlling the decay behaviour of k of WS-BrC in the South Asian outflow compared to the atmosphere over the Himalayan region. Choudhary et al.[116] indicated that photo-bleaching might have more significant impact than dilution on controlling the decay behaviour of k of WS-BrC in the South Asian outflow compared to the atmosphere over the Himalayan region. The observed differences in the relationships of k with the AAE underscore that absorption characteristics of BrC aerosols are not solely influenced by the kind of fuels and combustion conditions but also impacted by various atmospheric processes, such as the oxidation of organic compounds during long-distance transport. A study by Chen and Bond[73] also noted a similar relationship in aerosols derived from biofuel burning. This evidence suggests the complex absorption

nature of BrC. These findings highlight the importance of reconciling and refining the characterization of BrC optical properties based on actual atmospheric aerosols in comparison to results obtained under controlled laboratory conditions. Therefore, the results we found further point to the importance of considering atmospheric processes beyond direct emission sources when examining BrC optical properties.

3.4 Fractional absorption of BrC relative to EC and simple forcing efficiency

In order to understand the absorption contribution of BrC relative to EC, the fractional contribution of solar absorption by light-absorbing WSOC and OC at the Lachung site was evaluated as shown in Fig. 9. We found that the quantity of solar radiation absorbed by WS-BrC (MeS-BrC) in comparison to EC were 7.6 ± 5.4% (10.3 ± 5.1%), 5.3 ± 4.8% (7.1 ± 3.1%), 4 ± 1.4% (6.3 ± 2.2%) and 4 ± 1.6% (6.4 ± 1.3%) during spring, summer monsoon, autumn and winter, respectively. During our entire study period, WS-BrC and MeS-BrC absorption relative to EC at Lachung accounted for 5.2 ± 3.9% and 7.5 ± 3.5%. The higher fractional absorption of BrC observed at Lachung
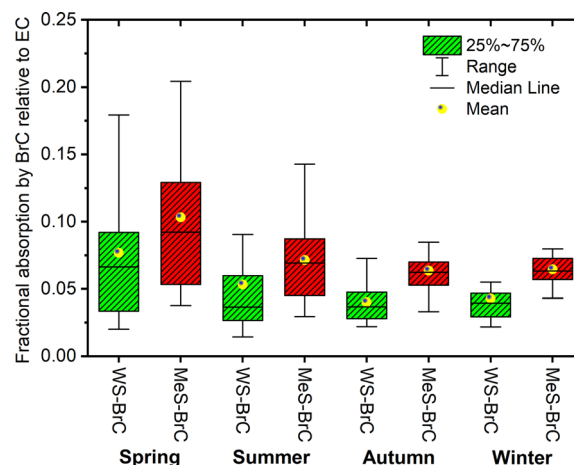

Fig. 9 Fractional solar absorption of WS-BrC and MeS-BrC relative to EC in aerosols at Lachung during the sampling period.

796 | Environ. Sci.: Atmos., 2024, **4**, 782–801

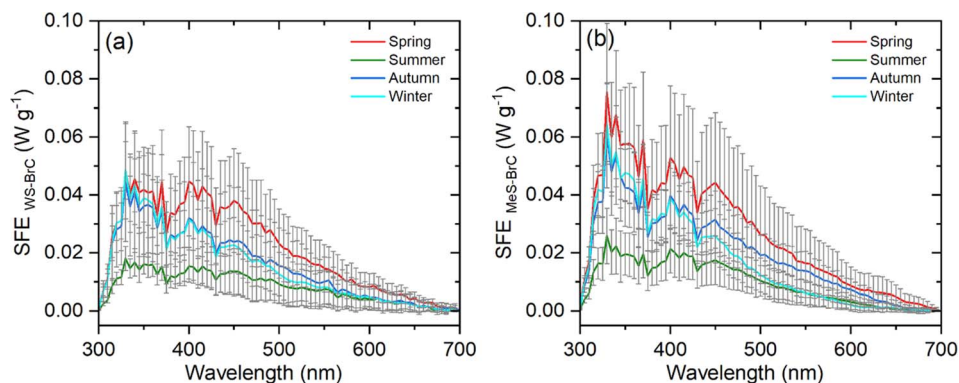© 2024 The Author(s). Published by the Royal Society of Chemistry

Fig. 10 Spectral variabilities of simple forcing efficiency (SFE) for (a) water-soluble BrC (WS-BrC) and (b) methanol-soluble BrC (MeS-BrC) aerosols.

specifically during spring indicated the significant contribution of transported anthropogenic sources in enhancing the BrC absorption in this remote part of the eastern Himalayas.

Earlier, Kirillova et al.[34] showed $4 \pm 1\%$ of solar radiation absorption by WS-BrC compared to EC, and $9 \pm 2\%$ by MeS-BrC relative to EC at a remote background site NCO-P, located at an altitude of about 5 km a.s.l., in the higher Himalayas. The differences in absorption by BrC at NCO-P and Lachung are mainly modulated by the altitudinal variations of these sites and distinct source processes even though both the sites are influenced by the long-range atmospheric transport of aerosols. Also, it should be noted here that, Zhao et al.[126] found that BrC concentration decreases more slowly than EC with altitude in the Himalayas and Tibetan Plateau region. The observed absorption by BrC aerosols of Lachung samples is found to be lower compared to the observations from the central IGP where BrC absorption accounts for 30% compared to that of EC,[18] and at Patiala in winter, where WS-BrC absorbed 40–55% of solar radiation, surpassing EC absorption.[62] These two sites were highly influenced by biomass burning emissions compared to Lachung. It is interesting to note that the relative absorption of BrC aerosols at Lachung is comparable to the observations from lower altitude continental sites in south Asia[61,99,117] as well as to the IGP outflow to the Indian ocean.[65] These comparative absorptions of BrC showed that the anthropogenic contributions to BrC absorption are relatively similar to those of these South Asian regions. This implies the significance of BrC aerosols as a light absorber in the higher Himalayas.

Fig. 10 shows the sensitivity study of the simple forcing efficiency (SFE) of WS-BrC and MeS-BrC aerosols at Lachung using the method proposed by Lei et al.[70] as described in Section 2.2. The average values of SFE of WS-BrC (MeS-BrC) aerosols were the highest during spring (WS-BrC: 8.7 ± 3.9 W g^{-1} and MeS-BrC: 10.8 ± 5.2 W g^{-1}) and lowest during summer (WS-BrC: 3.2 ± 1.6 W g^{-1} and MeS-BrC: 3.9 ± 1.8 W g^{-1}). These results show the substantial radiative effects of BrC aerosols on the eastern Himalayan region. Especially during spring, large-scale influence of biomass burning sources and chemical processing of organic aerosols is responsible for the enhanced absorption ability of BrC aerosols over this eastern Himalayan region.

Meanwhile, the local scale burning activities and photo-bleaching during winter are responsible for the lower absorption by BrC aerosols. The relatively significant absorption during autumn was contributed mainly by the post-agricultural burning activities, whereas the summertime BrC absorption was modulated mainly by photochemical oxidation processes. The substantial SFE values at Lachung suggest the significant radiative perturbations induced by the BrC aerosols over this remote eastern Himalayan region.

4. Conclusions and implications

We examined the light-absorbing characteristics of WS-BrC and MeS-BrC aerosols during March 2019 to February 2020 at Lachung, which is located in the remote high altitude eastern Himalayan region. Light absorption properties of water and methanol extracts revealed substantial evidence of BrC aerosol absorption in the atmosphere of the eastern Himalayan region with marked seasonal variabilities. The spring season demonstrated the highest levels of the absorption coefficients for both WS-BrC and MeS-BrC. Notably, MeS-BrC aerosols contributed almost 1.7 times higher absorption at 365 nm compared to the WS-BrC signifying the significant influence of BrC absorption due to water-insoluble BrC chromophores at the observational site. The correlation between b_{abs365} of WSOC (OC) and WS-BrC (MeS-BrC) indicated that BrC aerosols played a significant role in light absorption and had similar sources to WSOC and OC. Moreover, we found relatively higher correlation between b_{abs365} of WS-BrC and MeS-BrC and WSTN and WSON during spring and autumn, indicating the presence of nitrogenous organic chromophores in the BrC absorption during these periods.

The MAE$_{365}$ values ranged from 0.4 to 3.2 m^2 g^{-1} and 0.5–4.4 m^2 g^{-1} for WS-BrC and MeS-BrC, respectively, and are comparable with the previous measurements conducted at lower-altitude sites, implying a higher potential impact on climate in the high-altitude region. The elevated MAE$_{365}$ (1.5 ± 0.6 m^2 g^{-1} for WS-BrC and 2.07 ± 0.8 m^2 g^{-1} for MeS-BrC) values observed during spring suggest that organic aerosols undergo aqueous phase processing during long-range transport associated with intense biomass burning activities during this season,

© 2024 The Author(s). Published by the Royal Society of Chemistry

Environ. Sci.: Atmos., 2024, **4**, 782–801 | **797**

leading to increased light absorption. Solar radiation absorption by BrC relative to EC for the entire solar spectrum indicated $5.2 \pm 3.9\%$ absorption by WS-BrC and $7.5 \pm 3.5\%$ by MeS-BrC, which showed the significant contribution of BrC absorption by anthropogenic sources at this high-altitude Himalayan region. Our results provide significant contributions to comprehend the distinct absorption characteristics of BrC aerosols, which elucidated their role in the radiation budget in the eastern Himalayan region. Considering the possible climatic implications on Himalayan glaciers, it becomes imperative to focus specifically on the detailed molecular composition of BrC aerosols and their chemical transformations in future investigations. A deeper understanding of these factors can yield valuable knowledge regarding the climatic impacts of BrC aerosols and their potential contribution to glacier melt in this climate sensitive Himalayan region.

Conflicts of interest

The authors declare that they have no conflicts of interest.

Acknowledgements

References

1 D. Contini, R. Vecchi and M. Viana, *Atmosphere*, 2018, **9**, 181.

2 A. Christodoulou, I. Stavroulas, M. Vrekoussis, M. Desservettaz, M. Pikridas, E. Bimenyimana, J. Kushta, M. Ivančič, M. Rigler, P. Goloub, K. Oikonomou, R. Sarda-Estève, C. Savvides, C. Afif, N. Mihalopoulos, S. Sauvage and J. Sciare, *Atmos. Chem. Phys.*, 2023, **23**, 6431–6456.

3 A. Laskin, J. Laskin and S. A. Nizkorodov, *Chem. Rev.*, 2015, **115**, 4335–4382.

4 R. F. Hems, E. G. Schnitzler, C. Liu-Kang, C. D. Cappa and J. P. D. Abbatt, *ACS Earth Space Chem.*, 2021, **5**, 722–748.

5 U. Lohmann and J. Feichter, *Atmos. Chem. Phys.*, 2005, **5**, 715–737.

6 S. Huang, W. Hu, J. Chen, Z. Wu, D. Zhang and P. Fu, *Environ. Int.*, 2021, **146**, 106197.

7 I. Salma, A. Vasanits-Zsigrai, A. Machon, T. Varga, I. Major, V. Gergely and M. Molnár, *Atmos. Chem. Phys.*, 2020, **20**, 4295–4312.

8 R. K. Chakrabarty, N. J. Shetty, A. S. Thind, P. Beeler, B. J. Sumlin, C. Zhang, P. Liu, J. C. Idrobo, K. Adachi, N. L. Wagner, J. P. Schwarz, A. Ahern, A. J. Sedlacek, A. Lambe, C. Daube, M. Lyu, C. Liu, S. Herndon, T. B. Onasch and R. Mishra, *Nat. Geosci.*, 2023, **16**, 683–688.

9 D. Srivastava, T. V. Vu, S. Tong, Z. Shi and R. M. Harrison, *npj Clim. Atmos. Sci.*, 2022, **5**, 22.

10 T. Chen, P. Zhang, B. Chu, Q. Ma, Y. Ge, J. Liu and H. He, *npj Clim. Atmos. Sci.*, 2022, **5**, 95.

11 T. C. Bond, S. J. Doherty, D. W. Fahey, P. M. Forster, T. Berntsen, B. J. Deangelo, M. G. Flanner, S. Ghan, B. Kärcher, D. Koch, S. Kinne, Y. Kondo, P. K. Quinn, M. C. Sarofim, M. G. Schultz, M. Schulz, C. Venkataraman, H. Zhang, S. Zhang, N. Bellouin, S. K. Guttikunda, P. K. Hopke, M. Z. Jacobson, J. W. Kaiser, Z. Klimont, U. Lohmann, J. P. Schwarz, D. Shindell, T. Storelvmo, S. G. Warren and C. S. Zender, *J. Geophys. Res.: Atmos.*, 2013, **118**, 5380–5552.

12 J. Yan, X. Wang, P. Gong, C. Wang and Z. Cong, *Sci. Total Environ.*, 2018, **634**, 1475–1485.

13 R. K. Chakrabarty, H. Moosmüller, L. W. A. Chen, K. Lewis, W. P. Arnott, C. Mazzoleni, M. K. Dubey, C. E. Wold, W. M. Hao and S. M. Kreidenweis, *Atmos. Chem. Phys.*, 2010, **10**, 6363–6370.

14 Y. Cheng, K. B. He, M. Zheng, F. K. Duan, Z. Y. Du, Y. L. Ma, J. H. Tan, F. M. Yang, J. M. Liu, X. L. Zhang, R. J. Weber, M. H. Bergin and A. G. Russell, *Atmos. Chem. Phys.*, 2011, **11**, 11497–11510.

15 K. M. Updyke, T. B. Nguyen and S. A. Nizkorodov, *Atmos. Environ.*, 2012, **63**, 22–31.

16 S. H. Park, A. S. Panicker, D. I. Lee, W. S. Jung, S. M. Jang, M. Jang, D. Kim, Y. W. Kim and H. Jeong, *J. Atmos. Chem.*, 2010, **67**, 71–86.

17 B. Srinivas and M. M. Sarin, *Sci. Total Environ.*, 2014, **487**, 196–205.

18 P. M. Shamjad, S. N. Tripathi, N. M. Thamban and H. Vreeland, *Sci. Rep.*, 2016, **6**, 37735.

19 R. Satish and N. Rastogi, *ACS Omega*, 2019, **4**, 1814–1853.

20 G. Wu, K. Ram, P. Fu, W. Wang, Y. Zhang, X. Liu, E. A. Stone, B. B. Pradhan, P. M. Dangol, A. K. Panday, X. Wan, Z. Bai, S. Kang, Q. Zhang and Z. Cong, *Environ. Sci. Technol.*, 2019, **53**, 3471–3479.

21 F. Jiang, J. Song, J. Bauer, L. Gao, M. Vallon, R. Gebhardt, T. Leisner, S. Norra and H. Saathoff, *Atmos. Chem. Phys.*, 2022, **22**, 14971–14986.

22 T. Nakayama, K. Sato, Y. Matsumi, T. Imamura, A. Yamazaki and A. Uchiyama, *Atmos. Chem. Phys.*, 2013, **13**, 531–545.

23 M. Zhong and M. Jang, *Atmos. Chem. Phys.*, 2014, **14**, 1517–1525.

24 W. Marrero-Ortiz, M. Hu, Z. Du, Y. Ji, Y. Wang, S. Guo, Y. Lin, M. Gomez-Hermandez, J. Peng, Y. Li, J. Secrest, M. L. Zamora, Y. Wang, T. An and R. Zhang, *Environ. Sci. Technol.*, 2019, **53**, 117–126.

25 K. Siemens, A. Morales, Q. He, C. Li, A. P. S. Hettiyadura, Y. Rudich and A. Laskin, *Environ. Sci. Technol.*, 2022, **56**, 3340–3353.

798 | *Environ. Sci.: Atmos.*, 2024, **4**, 782–801

© 2024 The Author(s). Published by the Royal Society of Chemistry

26 A. Zhang, Y. Wang, Y. Zhang, R. J. Weber, Y. Song, Z. Ke and Y. Zou, *Atmos. Chem. Phys.*, 2020, **20**, 1901–1920.

27 Y. Zhu, Q. Wang, X. Yang, N. Yang and X. Wang, *Atmosphere*, 2021, **12**, 892.

28 Q. Yuan, J. Xu, L. Liu, A. Zhang, Y. Liu, J. Zhang, X. Wan, M. Li, K. Qin, Z. Cong, Y. Wang, S. Kang, Z. Shi, M. Posfai and W. Li, *Environ. Sci. Technol. Lett.*, 2021, **8**(1), 16–23.

29 L. T. Fleming, P. Lin, J. M. Roberts, V. Selimovic, R. Yokelson, J. Laskin, A. Laskin and S. A. Nizkorodov, *Atmos. Chem. Phys.*, 2020, **20**, 1105–1129.

30 T. Bolch, A. Kulkarni, A. Kääb, C. Huggel, F. Paul, J. G. Cogley, H. Frey, J. S. Kargel, K. Fujita, M. Scheel, S. Bajracharya and M. Stoffel, *Science*, 2012, **336**, 310–314.

31 F. Brun, E. Berthier, P. Wagnon, A. Kääb and D. Treichler, *Nat. Geosci.*, 2017, **10**, 668–673.

32 S. Kang, Y. Zhang, Y. Qian and H. Wang, *Earth-Sci. Rev.*, 2020, **210**, 103346.

33 K. H. Usha, V. S. Nair and S. S. Babu, *Water Resour. Res.*, 2022, **58**, e2021WR030140.

34 E. N. Kirillova, S. Fuzzi and S. Decesari, *J. Geophys. Res.*, 2016, 9621–9639.

35 S. S. Babu, J. P. Chaubey, K. K. Moorthy, M. M. Gogoi, S. K. Kompalli, V. Sreekanth, S. P. Bagare, B. C. Bhatt, V. K. Gaur, T. P. Prabhu and N. S. Singh, *J. Geophys. Res.*, 2011, **116**, 1–15.

36 S. K. Kompalli, S. Suresh Babu, L. N. Bharatan and K. Krishna Moorthy, *Curr. Sci.*, 2016, **111**, 117–131.

37 P. S. Negi, C. P. Pandey and N. Singh, *Atmos. Environ.*, 2019, **214**, 116879.

38 M. M. Gogoi, S. S. Babu, B. S. Arun, K. K. Moorthy, A. Ajay, P. Ajay, A. Suryavanshi, A. Borgohain, A. Guha, A. Shaikh, B. Pathak, B. Gharai, B. Ramasamy, G. Balakrishnaiah, H. B. Menon, J. C. Kuniyal, J. Krishnan, K. R. Gopal, M. Maheshwari, M. Naja, P. Kaur, P. K. Bhuyan, P. Gupta, P. Singh, P. Srivastava, R. S. Singh, R. Kumar, S. Rastogi, S. S. Kundu, S. K. Kompalli, S. Panda, T. C. Rao, T. Das and Y. Kant, *Curr. Sci.*, 2021, 341–351.

39 R. C. Thakur, B. S. Arun, M. M. Gogoi, M. Thamban, R. J. Thayyen, B. L. Redkar and S. S. Babu, *Atmos. Environ.*, 2021, **261**, 118564.

40 T. H. Painter, A. C. Bryant and S. McKenzie Skiles, *Geophys. Res. Lett.*, 2012, **39**, 1–7.

41 B. S. Arun, A. R. Aswini, M. M. Gogoi, P. Hegde, S. Kumar Kompalli, P. Sharma and S. Suresh Babu, *Atmos. Environ.*, 2019, **218**, 117017.

42 G. Wu, X. Wan, S. Gao, P. Fu, Y. Yin, G. Li, G. Zhang, S. Kang, K. Ram and Z. Cong, *Environ. Sci. Technol.*, 2018, **52**, 7203–7211.

43 Q. Yuan, X. Wan, Z. Cong, M. Li, L. Liu, S. Shu, R. Liu, L. Xu, J. Zhang, X. Ding and W. Li, *J. Geophys. Res.: Atmos.*, 2020, **125**, e2020JD032615.

44 C. S. Zhu, J. J. Cao, R. J. Huang, Z. X. Shen, Q. Y. Wang and N. N. Zhang, *Sci. Total Environ.*, 2018, **625**, 246–251.

45 L. Zhu, X. Lü, J. Wang, P. Peng, T. Kaspe, G. Daut, T. Haberzettl, P. Frenzel, Q. Li, R. Yang, A. Schwalb and R. Mäusbacher, *Sci. Rep.*, 2015, **5**, 13318.

46 Z. Ma, Y. Xu, J. Peng, Q. Chen, D. Wan, K. He, Z. Shi and H. Li, *Int. J. Remote Sens.*, 2018, **39**(12), 3891–3907.

47 T. Bolch, J. M. Shea, S. Liu, F. M. Azam, Y. Gao, S. Gruber, W. W. Immerzeel, A. Kulkarni, H. Li, A. A. Tahir, G. Zhang and Y. Zhang, *The Hindu Kush Himalaya Assessment*, Springer, 2019, pp. 209–245.

48 G. Li, Z. Yu, W. Wang, Q. Ju and X. Chen, *Atmos. Res.*, 2021, **247**, 105259.

49 K. H. Usha, V. S. Nair and S. S. Babu, *J. Geophys. Res.: Atmos.*, 2022, **127**, e2021JD036384.

50 R. Ravindra, A. V. Kulkarni, A. P. Dimri, K. Sain, M. C. Sharma, A. Banerjee, P. Sharma, T. Meloth, I. Rashid and N. C. Pant, *Proc. Indian Natl. Sci. Acad.*, 2024, 2454–9983.

51 B. S. Arun, M. M. Gogoi, A. Borgohain, P. Hegde, S. S. Kundu and S. S. Babu, *Atmos. Res.*, 2021, **263**, 105799.

52 B. S. Arun, M. M. Gogoi, P. Hegde, A. Borgohain, S. K. R. Boreddy, S. S. Kundu and S. S. Babu, *ACS Earth Space Chem.*, 2021, **5**, 2493–2506.

53 H. J. Fowler and D. R. Archer, *J. Clim.*, 2006, **19**(17), 4276–4293.

54 E. Lee, J. L. Carrivick, D. J. Quincey, S. J. Cook, W. H. M. James and L. E. Brown, *Sci. Rep.*, 2021, **11**(24284), 2045–2322.

55 A. Jouberton, T. E. Shaw, E. Miles, M. McCarthy, S. Fugger, S. Ren, A. Dehecq, W. Yang and F. Pellicciotti, *Proc. Natl. Acad. Sci. U.S.A.*, 2022, **119**, 37.

56 J. M. Maurer, S. B. Rupper and J. M. Schaefer, *Cryosphere*, 2016, **10**, 2203–2215.

57 A. V. Kulkarni, S. S. Tejal, A. Kulkarni, H. S. Negi, I. M. Bahuguna and M. Thamban, *Water Secur.*, 2021, **14**, 100101.

58 C. Wu, G. Wang, J. Li, J. Li, C. Cao, S. Ge, Y. Xie, J. Chen, X. Li, G. Xue, X. Wang, Z. Zhao and F. Cao, *Atmos. Chem. Phys.*, 2020, **20**, 2017–2030.

59 D. Paraskevopoulou, S. Bikkina, G. Grivas, D. G. Kaskaoutis, M. Tsagkaraki, K. Tavernaraki and N. Mihalopoulos, *MethodsX*, 2023, **11**, 102313.

60 D. Paraskevopoulou, D. G. Kaskaoutis, G. Grivas, S. Bikkina, M. Tsagkaraki, I. M. Vrettou, K. Tavernaraki, K. Papoutsidaki, I. Stavroulas, E. Liakakou, A. Bougiatioti, K. Oikonomou, E. Gerasopoulos and N. Mihalopoulos, *Sci. Total Environ.*, 2023, **860**, 160434.

61 E. N. Kirillova, A. Andersson, J. Han, M. Lee and Ö. Gustafsson, *Atmos. Chem. Phys.*, 2014, **14**, 1413–1422.

62 B. Srinivas, N. Rastogi, M. M. Sarin, A. Singh and D. Singh, *Atmos. Environ.*, 2016, **125**, 360–370.

63 Y. Cheng, K. He, Z. Du, G. Engling, J. Liu, Y. Ma, M. Zheng and R. J. Weber, *Atmos. Environ.*, 2016, **127**, 355–364.

64 F. Yan, S. Kang, M. Sillanpää, Z. Hu, S. Gao, P. Chen, S. Gautam, S.-P. Reinikainen and C. Li, *Environ. Pollut.*, 2020, **262**, 114300.

65 S. Bikkina and M. Sarin, *Environ. Sci.: Processes Impacts*, 2019, **21**, 970–987.

66 J. Liu, M. Bergin, H. Guo, L. King, N. Kotra, E. Edgerton and R. J. Weber, *Atmos. Chem. Phys.*, 2013, **13**, 12389–12404.

67 R. Levinson, H. Akbari and P. Berdahl, *Sol. Energy*, 2010, **84**, 1717–1744.

© 2024 The Author(s). Published by the Royal Society of Chemistry

Environ. Sci.: Atmos., 2024, **4**, 782–801 | **799**

68 A. K. Alang, S. G. Aggarwal, K. Singh, D. Soni and P. Hegde, *Atmos. Res.*, 2023, **296**, 107073.

69 K. Ram and M. M. Sarin, *Environ. Sci. Technol.*, 2009, **43**(21), 8233–8239.

70 Y. Lei, Z. Shen, T. Zhang, Q. Zhang, Q. Wang, J. Sun, X. Gong, J. Cao, H. Xu, S. Liu and L. Yang, *Sci. Total Environ.*, 2018, **622–623**, 244–251.

71 K. G. Karlsson, A. Riihelä, J. Trentmann, M. Stengel, I. Solodovnik, J. F. Meirink, A. Devasthale, E. Jääskeläinen, V. Kallio-Myers, S. Eliasson, N. Benas, E. Johansson, D. Stein, S. Finkensieper, N. Håkansson, T. Akkermans, N. Clerbaux, N. Selbach, M. Schröder and R. Hollmann, *Earth Syst. Sci. Data*, 2023, **15**, 4901–4926.

72 S. K. R. Boreddy, P. Hegde, B. S. Arun, A. R. Aswini and S. S. Babu, *Sci. Total Environ.*, 2022, **845**, 157163.

73 Y. Chen and T. C. Bond, *Atmos. Chem. Phys.*, 2010, **10**, 1773–1787.

74 P. Chen, S. Kang, C. Li, M. Rupakheti, F. Yan, Q. Li, Z. Ji, Q. Zhang, W. Luo and M. Sillanpää, *Sci. Total Environ.*, 2015, **538**, 86–92.

75 S. Izhar, T. Gupta and A. K. Panday, *Environ. Pollut.*, 2020, **263**, 114640.

76 A. Rana, S. Dey, P. Rawat, A. Mukherjee, J. Mao, S. Jia, P. S. Khillare, A. K. Yadav and S. Sarkar, *Sci. Total Environ.*, 2020, **716**, 137102.

77 A. Hecobian, X. Zhang, M. Zheng, N. Frank, E. S. Edgerton and R. J. Weber, *Atmos. Chem. Phys.*, 2010, **10**, 5965–5977.

78 S. Li, M. Zhu, W. Yang, M. Tang, X. Huang, Y. Yu, H. Fang, X. Yu, Q. Yu, X. Fu, W. Song, Y. Zhang, X. Bi and X. Wang, *Sci. Total Environ.*, 2018, **633**, 1360e1369.

79 B. Srinivas and M. M. Sarin, *Environ. Res. Lett.*, 2013, **8**, 044042.

80 C. Bosch, A. Andersson, E. N. Kirillova, K. Budhavant, S. Tiwari, P. S. Praveen, L. M. Russell, N. D. Beres, V. Ramanathan and Ö. Gustafsson, *J. Geophys. Res.: Atmos.*, 2014, **119**(11), 743–759.

81 P. M. Shamjad, S. N. Tripathi, R. Pathak, M. Hallquist, A. Arola and M. H. Bergin, *Environ. Sci. Technol.*, 2015, **49**, 10474–10481.

82 Y. Cheng, K. He, G. Engling, R. Weber, J. Liu, Z. Du and S. Dong, *Sci. Total Environ.*, 2017, **599–600**, 1047–1055.

83 X. Zhang, Y. H. Lin, J. D. Surratt and R. J. Weber, *Environ. Sci. Technol.*, 2013, **47**, 3685–3693.

84 E. Soleimanian, A. Mousavi, S. Taghvaee, M. M. Shafer and C. Sioutas, *Sci. Total Environ.*, 2021, **705**, 135902.

85 R. J. Huang, L. Yang, J. Cao, Y. Chen, Q. Chen, Y. Li, J. Duan, C. Zhu, W. Dai, K. Wang, C. Lin, H. Ni, J. C. Corbin, Y. Wu, R. Zhang, X. Tie, T. Hoffmann, C. O'Dowd and U. Dusek, *Environ. Sci. Technol.*, 2018, **52**, 6825–6833.

86 S. Dasari, A. Andersson, S. Bikkina, H. Holmstrand, K. Budhavant, S. Satheesh, E. Asmi, J. Kesti, J. Backman, A. Salam, D. S. Bisht, S. Tiwari, Z. Hameed and Ö. Gustafsson, *Sci. Adv.*, 2019, **5**, eaau8066.

87 J. Yang, W. Xu and H. Cheng, *Atmosphere*, 2018, **9**, 1–9.

88 H. Kim, J. Y. Kim, H. C. Jin, J. Y. Lee and S. P. Lee, *Atmos. Environ.*, 2016, **129**, 234–242.

89 L. Zeng, J. Dibb, E. Scheuer, J. M. Katich, J. P. Schwarz, I. Bourgeois, J. Peischl, T. Ryerson, C. Warneke, A. E. Perring, G. S. Diskin, J. P. DiGangi, J. B. Nowak, R. H. Moore, E. B. Wiggins, D. Pagonis, H. Guo, P. Campuzano-Jost, J. L. Jimenez, L. Xu and R. J. Weber, *Atmos. Chem. Phys.*, 2022, **22**, 8009–8036.

90 P. Lin, L. T. Fleming, S. A. Nizkorodov, J. Laskin and A. Laskin, *Anal. Chem.*, 2018, 12493–12502.

91 D. G. Kaskaoutis, G. Grivas, K. Oikonomou, P. Tavernaraki, K. Papoutsidaki, M. Tsagkaraki, I. Stavroulas, P. Zarmpas, D. Paraskevopoulou, A. Bougiatioti, E. Liakakou, M. Gavrouzou, U. C. Dumka, N. Hatzianastassiou, J. Sciare, E. Gerasopoulos and N. Mihalopoulos, *Atmos. Environ.*, 2022, **280**, 119139.

92 A. Rai, S. Mukherjee, A. Chatterjee, N. Choudhary, G. Kotnala, T. K. Mandal and S. K. Sharma, *Aerosp. Eng.*, 2020, **4**, 26–40.

93 S. Gilardoni, P. Massoli, L. Giulianelli, M. Rinaldi, M. Paglione, F. Pollini, C. Lanconelli, V. Poluzzi, S. Carbone, R. Hillamo, L. M. Russell, M. C. Facchini and S. Fuzzi, *Atmos. Chem. Phys.*, 2014, **14**, 6967–6981.

94 B. Ervens, B. J. Turpin and R. J. Weber, *Atmos. Chem. Phys.*, 2011, **11**, 11069–11102.

95 J. P. S. Wong, M. Tsagkaraki, I. Tsiodra, N. Mihalopoulos, K. Violaki, M. Kanakidou, J. Sciare, A. Nenes and R. J. Weber, *Atmos. Chem. Phys.*, 2019, **19**, 7319–7334.

96 V. Choudhary, M. L. Roson, X. Guo, T. Gautam, T. Gupta and R. Zhao, *Environ. Sci.: Atmos.*, 2023, **3**, 816.

97 R. Saleh, C. J. Hennigan, G. R. McMeeking, W. K. Chuang, E. S. Robinson, H. Coe, N. M. Donahue and A. L. Robinson, *Atmos. Chem. Phys.*, 2013, **13**, 7683–7693.

98 P. Lin, N. Bluvshtein, Y. Rudich, S. A. Nizkorodov, J. Laskin and A. Laskin, *Environ. Sci. Technol.*, 2017, **51**, 11561–11570.

99 P. Chen, S. Kang, L. Tripathee, K. Ram, M. Rupakheti, A. K. Panday, Q. Zhang, J. Guo, X. Wang, T. Pu and C. Li, *Environ. Pollut.*, 2020, **261**, 114239.

100 N. Bluvshtein, P. Lin, J. M. Flores, L. Segev, Y. Mazar, E. Tas, G. Snider, C. Weagle, S. S. Brown, A. Laskin and Y. Rudich, *J. Geophys. Res.: Atmos.*, 2017, **122**, 5441–5456.

101 Z. Guo, Y. Yang, X. Hu, X. Peng, Y. Fu, W. Sun, G. Zhang, D. Chen, X. Bi, X. Wang and P. Peng, *Atmos. Chem. Phys.*, 2020, **22**, 4827–4839.

102 C. Sarkar, C. Venkataraman, S. Yadav, H. C. Phuleria and A. Chatterjee, *Environ. Pollut.*, 2019, **254**, 113077.

103 R. Satish, N. Rastogi, A. Singh and D. Singh, *Environ. Sci. Pollut. Res.*, 2020, **27**, 33339–33350.

104 R. R. Draxler and G. D. Rolph, *HYSPLIT (HYbrid Single-Particle Lagrangian Integrated Trajectory) Model access via NOAA ARL READY*, NOAA Air Resources Laboratory, Silver Spring, 2013.

105 P. Bonasoni, P. Cristofanelli, A. Marinoni, E. Vuillermoz and B. Adhikari, *Mt. Res. Dev.*, 2012, **32**, 468–479.

106 P. Bonasoni, P. Laj, A. Marinoni, M. Sprenger, F. Angelini, J. Arduini, U. Bonafè, F. Calzolari, T. Colombo, S. Decesari, C. Di Biagio, A. G. Di Sarra, F. Evangelisti, R. Duchi, M. C. Facchini, S. Fuzzi, G. P. Gobbi, M. Maione, A. Panday, F. Roccato, K. Sellegri, H. Venzac,

800 | *Environ. Sci.: Atmos.*, 2024, **4**, 782–801

© 2024 The Author(s). Published by the Royal Society of Chemistry

G. P. Verza, P. Villani, E. Vuillermoz and P. Cristofanelli, *Atmos. Chem. Phys.*, 2010, **10**, 7515–7531.

107 E. N. Kirillova, A. Andersson, R. J. Sheesley, M. Krusa, P. S. Praveen, K. Budhavant, P. D. Safai, P. S. P. Rao and Ö. Gustafsson, *J. Geophys. Res.: Atmos.*, 2013, **118**, 614–626.

108 C.-S. Zhu, Y. Qu, H. Huang, J. Chen, W.-T. Dai, R.-J. Huang and J.-J. Cao, *Geophys. Res. Lett.*, 2021, **48**, e2021GL092524.

109 Q. Wang, Y. Han, J. Ye, S. Liu, S. Pongpiachan, N. Zhang, Y. Han, J. Tian, C. Wu, X. Long, Q. Zhang, W. Zhang, Z. Zhao and J. Cao, *Geophys. Res. Lett.*, 2019, **46**, 4962–4970.

110 S. Gilardoni, P. Massoli, M. Paglione, L. Giulianelli, C. Carbone, M. Rinaldi, S. Decesari, S. Sandrini, F. Costabile, G. P. Gobbi, M. C. Pietrogrande, M. Visentin, F. Scotto, S. Fuzzi and M. C. Facchini, *Proc. Natl. Acad. Sci. U. S. A.*, 2016, **113**, 10013–10018.

111 R. F. Hems, E. G. Schnitzler, M. Bastawrous, R. Soong, A. J. Simpson and J. P. D. Abbatt, *ACS Earth Space Chem.*, 2020, **4**, 1149–1160.

112 L. Yu, J. Smith, A. Laskin, C. Anastasio, J. Laskin and Q. Zhang, *Atmos. Chem. Phys.*, 2014, **14**, 13801–13816.

113 J. D. Smith, H. Kinney and C. Anastasio, *Atmos. Environ.*, 2016, **126**, 36–44.

114 C. Cheng, G. Wang, J. Meng, Q. Wang, J. Cao, J. Li and J. Wang, *Atmos. Res.*, 2015, **161–162**, 134–142.

115 G. Wu, X. Wan, K. Ram, P. Li, B. Liu, Y. Yin, P. Fu, M. Loewen, S. Gao, S. Kang, K. Kawamura, Y. Wang and Z. Cong, *Environ. Pollut.*, 2020, **257**, 113616.

116 V. Choudhary, T. Gupta and R. Zhao, *ACS Earth Space Chem.*, 2022, **6**(10), 2335–2347.

117 E. N. Kirillova, A. Andersson, S. Tiwari, A. K. Srivastava, D. S. Bisht and Ö. Gustafsson, *J. Geophys. Res.*, 2014, **119**, 3476–3485.

118 Z. Shen, Q. Zhang, J. Cao, L. Zhang, Y. Lei, Y. Huang, R.-J. Huang, J. Gao, Z. Zhao, C. Zhu, X. Yin, C. Zheng, H. Xu and S. Liu, *Atmos. Environ.*, 2017, **150**, 322–330.

119 C. Li, F. Yan, S. Kang, C. Yan, Z. Hu, P. Chen, S. Gao, C. Zhang, C. He, S. Kaspari and A. Stubbins, *Environ. Int.*, 2021, **146**, 106281.

120 P. Chen, S. Kang, L. Tripathee, A. K. Panday, M. Rupakheti, D. Rupakheti, Q. Zhang, J. Guo, C. Li and T. Pu, *Environ. Sci. Pollut. Res.*, 2020, **27**, 10617–10628.

121 R. J. Huang, L. Yang, J. Shen, W. Yuan, Y. Gong, J. Guo, W. Cao, J. Duan, H. Ni, C. Zhu, W. Dai, Y. Li, Y. Chen, Q. Chen, Y. Wu, R. Zhang, U. Dusek, C. O'Dowd and T. Hoffmann, *Environ. Sci. Technol.*, 2020, **54**(13), 7836–7847.

122 Y. Chen, X. Ge, H. Chen, X. Xie, Y. Chen, J. Wang, Z. Ye, M. Bao, Y. Zhang and M. Chen, *Atmos. Environ.*, 2018, **187**, 230–240.

123 R. Saleh, M. Marks, J. Heo, P. J. Adams, N. M. Donahue and A. L. Robinson, *J. Geophys. Res.: Atmos.*, 2015, **120**, 10285–10296.

124 R. P. Pokhrel, N. L. Wagner, J. M. Langridge, D. A. Lack, T. Jayarathne, E. A. Stone, C. E. Stockwell, R. J. Yokelson and S. M. Murphy, *Atmos. Chem. Phys.*, 2016, **16**, 9549–9561.

125 P. M. Shamjad, R. V. Satish, N. M. Thamban, N. Rastogi and S. N. Tripathi, *ACS Earth Space Chem.*, 2018, **2**, 31–37.

126 S. Zhao, S. Qi, Y. Yu, S. Kang, L. Dong, J. Chen and D. Yin, *Atmos. Chem. Phys.*, 2022, **22**, 14693–14708.